LAMONT-DOHERTY GEOLOGICAL OBSERVATORY

OF COLUMBIA UNIVERSITY

PALISADES, NEW YORK

(1) OCEAN CURRENT OBSERVATIONS AT THE AIDJEX 1972 MAIN CAMP
by Kenneth Hunkins and Myron Fliegel

(2) THE OCEANIC BOUNDARY LAYER AND ICE-WATER STRESS DURING AIDJEX 1972 by Kenneth Hunkins

(3) AN ESTIMATE OF INTERNAL WAVE DRAG ON PACK ICE
by Kenneth Hunkins

CU-1-74 Technical Report No. 1

Department of the Navy
Office of Naval Research
Contract N00014-67-A-0108-0039
Task Number NR307-359 Project No. 461

December, 1974

OCEAN CURRENT OBSERVATIONS AT THE AIDJEX 1972 MAIN CAMP

by

Kenneth Hunkins and Myron Fliegel
Lamont-Doherty Geological Observatory
Columbia University, Palisades, New York 10964

ABSTRACT

During the 1972 AIDJEX pilot study, mast-mounted current meters were operated continuously for 30 days in the main camp to measure currents at ten depths between 2 m and 100 m below the ice base. The currents were plotted in three forms: relative speed and direction, absolute speed and direction, and progressive vector.

INTRODUCTION

The primary aim of the AIDJEX oceanographic program is the determination of water drag on the base of drifting pack ice. During the AIDJEX pilot program in 1972, ocean currents were monitored continuously at ten levels between the surface and 100 m. This report describes the experimental techniques and data reduction and summarizes the results. An accompanying article in this Bulletin applies these results to water drag.

A secondary objective of the oceanographic program is to explore basic processes in the upper layers of the Arctic Ocean. The current observations presented here and those from the 1971 pilot program have contributed to a better understanding of two phenomena in the upper layers: sub-ice boundary currents and subsurface baroclinic eddies. The sub-ice boundary currents were seen most clearly in the 1971 data and are apparently convection cells driven by brine production during freezing. Subsurface eddies were most clearly observed in the 1972 data presented here. The eddies are 10-20 km in diameter and are found between depths of 50 and 300 m. Speeds may reach 40 cm/sec at the core level, 150 m. These eddies may play an

important part in the horizontal exchange of heat, momentum, and salt between the Arctic Ocean and adjoining seas. Details of the eddies are given in a separate report [Hunkins, 1974].

DATA ACQUISITION

Current meters were suspended on inverted masts with their orientation rigidly fixed to that of the floe on which the station was situated. The current meters (Bendix/Marine Advisers Q-9) were of the Savonius rotor type. Although these meters have a magnetic compass for direction reference, the compasses were locked by a magnet attached to the exterior of the instrument. Current direction was thus referenced to the floe itself. The azimuth of the floe was monitored daily with celestial observations.

The threshhold sensitivity of the current meters is conservatively estimated by the manufacturer as 2.6 cm/sec, although our experience indicates that the threshhold may be considerably lower. The manufacturer's calibration curve was used for rotor turns versus water speed. It is a general conclusion of most tests on Savonius rotor meters that this is satisfactory for meters manufactured with adequate quality control so long as the bearings are free. The bearings were checked for clearance before launching the instruments by observing rotor spindown in air. Directional accuracy is specified as ±3° by the manufacturer. The current meters weigh 34 pounds in air and 22 pounds in water. Bolted fittings attached the masts to the flanges on the top and bottom of the instruments. The instruments were axially aligned with the mast, forming an extension of it, so that no supports interfered with flow.

Three masts were used to support the ten current meters. Meters were placed on the shallow mast at levels of 2, 4, 8, 12, and 20 m below the ice base. All current meter depths were referenced to the bottom of the ice, nominally taken as 2 m below sea level. (For depth below sea level, add 2 m to indicated depths.) Ice thickness was measured at four locations by the CRREL group around the current meter building. They found ice thicknesses of 2.26, 2.04, 2.11, and 2.08 m below sea level. Meters

were suspended at 30, 40, and 50 m on the intermediate mast and at 70 and 100 m on the deep mast.

The shallow mast, a prototype of the ones to be used in the 1975 experiment, was made of one-inch stainless steel tubing fitted with locking swivel attachments for alignment of individual meters. The intermediate and deep masts were of 1¼" aluminum pipe locked together with collars and pins. Individual instruments were not aligned on the aluminum masts, but their orientations relative to each other were measured. Proper alignment along all masts was assured by punch marks on the tubing or pipe applied in a lathe bed.

The shallow and intermediate masts were installed through separate ice wells 2 m apart in the current meter building; the deep mast was located 30 m away in the Lamont living quarters. The top of each mast emerged to eye level in the buildings and was fitted with an azimuth plate for alignment. Surveys run with a theodolite tied the mast alignment to the floe azimuth.

Signals, carried from the sensors to the surface by electrical cables, were converted to analog voltages by signal conditioners (Bendix/Marine Advisers S-11). Speed and direction at all ten levels were displayed continuously on panel meters in the current meter building during the experiment. The data were recorded on paper strip charts with multipoint servo recorders which printed once per minute on magnetic tape. The digital data acquisition system (Hewlett Packard Model 2012D) included a reed scanner, integrating digital voltmeter, coupler, and incremental magnetic tape recorder. The signal conditioners had a response time of about 30 seconds for the speed channel and 10 seconds for the direction, so that the problem of aliasing high-frequency fluctuations with a one-minute sampling interval should be negligible. The chart recorders operated from 15 March to 26 April, but a failure in the tape recorder delayed the start of digital recording to 28 March. The digital data, essentially complete through the inclusive dates of 29 March to 25 April, are the data described here.

The entire system, except for the current sensors themselves, was calibrated at the beginning, the middle, and the end of the experiment.

Calibration signals were introduced into the signal conditioners and monitored on the chart recorders and digital voltmeter. A precision decade resistance box was used to simulate direction changes of the vane and potentiometer in the actual direction sensor. A square-wave generator simulated output of the magnetic reed switch in the actual speed sensor. The data were corrected on the basis of the calibrations during processing after the field study.

Since the ocean currents are observed from a moving platform, a knowledge of ice drift is required for complete interpretation of the results. Ice position was monitored at irregular intervals of roughly one hour with a U. S. Navy satellite navigation system. The position data were smoothed with a Kalman filter with a response of 50% at a period of 14 hours. The slope of the Kalman filter is somewhat steeper than that of a cosine filter. Details of the treatment of the navigation data are given by Thorndike [1973].

Smoothed ice speed and direction are shown in Figure 1. Since these data have been filtered, it is of interest to know if higher-frequency

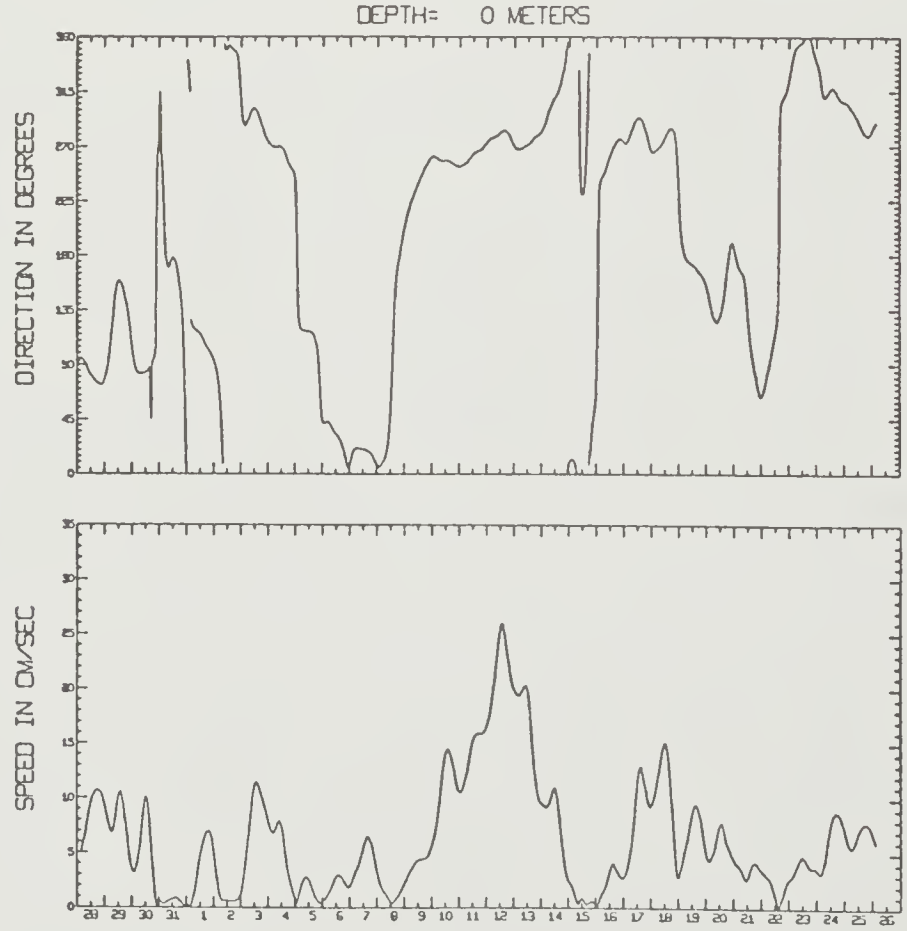

Fig. 1. Smoothed ice speed and direction, AIDJEX main camp, 1972.

motions of the ice have been suppressed. To check this point, positions were taken over a period of ten days with an acoustic bottom reference system for comparison with the satellite navigation. The acoustic system yields highly precise position relative to a bottom transponder at intervals of a few minutes. Combined data, incorporating both satellite and acoustic results, presumably represent ice motion of all periods in all essential detail. These combined data were compared with the satellite data alone. The variance of the difference between the two time series was 1000 m^2 hr^{-2} for the east component and 650 for the north. This indicates that the ice velocities are reliable to better than 1 cm/sec.

Inspection of the data plot of Thorndike reveals that much of the variance is associated with oscillations with a period of about 12 hours. This is probably due to inertial oscillations of the ice, which are suppressed by the smoothing. For some purposes, 12-hour means of ice velocity have been used to eliminate these oscillations.

DATA REDUCTION

The data tapes written by the digital data system are formatted BCD tapes that can be read by many computers. Since all the current meter data were to be reduced on a single computer (IBM 1130), the tapes were rewritten in unformatted arrays. This reduced the amount of magnetic tape used from two full 2400-foot reels to about half a reel, with considerable savings in computer access time. These data were expressed in volts, the original field unit. The calibration results were then used to convert the data into speed in cm/sec and degrees from true north. The final tape record contains data in 21 channels: 10 speed channels, 10 direction channels, and a time channel.

Since the data were recorded at one-minute intervals for almost a month, there are more than 40,000 data points per channel. This number was reduced considerably by filtering the data with an 80-minute rectangular filter and sampling every hour. Each hourly value thus represents an average of the preceding and the succeeding 40 minutes. These filtered data

were recorded on disk files to provide rapid random access. The one-minute data have not been used since they were filtered, but the magnetic tapes are still available for studying high-frequency phenomena.

Ice velocity at one-hour intervals was also recorded on disk. These data were then added vectorially to the data for currents measured relative to the ice motion. The true currents thus obtained were also written on disk. The disk therefore contains three types of data, each sampled hourly: ice velocity, relative current velocity at ten depths, and true velocity at ten depths. These are the data sets that have been used to construct the figures and tables in this report.

DATA PRESENTATION

Ocean currents in general form a three-dimensional vector field that changes continuously with time. The current meters used in AIDJEX measured only horizontal currents. Vertical currents are usually several orders of magnitude less than horizontal currents in the ocean. The AIDJEX data are thus two-dimensional vectors in time at discrete levels in the ocean. The location of the measuring site varies with time as the ice station drifts. The station drifted generally westward at a rate of about 2 km/day. At the beginning of digital recording on 29 March the station was at 75°03'N 148°43'W; at the end, on 25 April, it was at 75°06'N 151°32'W. The observations are thus neither exactly in an Eulerian nor exactly in a Lagrangian frame of reference. The first would be from a point fixed relative to the ocean floor, and the second would follow the path of a water particle.

Since a time-varying vector field involves four dimensions, it cannot be simply depicted on a two-dimensional page. Presentations of current data are compromises, and some presentations are better than others for emphasizing particular aspects of current behavior. From the many possibilities, two types of presentation were selected for use here. The first, current speed and direction, either relative or absolute, plotted against time, emphasizes such time-varying current features as tides, inertial oscillations, and storm effects. The second presentation, progressive vector diagrams representing

the displacement of a water particle provided that the currents are unchanging horizontally, emphasizes the net displacement of a water particle or the mean current.

The quantities actually measured were current speed and direction relative to the ice at ten levels. The relative currents are shown in Figures 2-11. Note that the times in these diagrams and in all others in this paper are Alaskan Standard Time, where AST = GMT - 10 hours. Direction is referenced to true north.

The relative current plots provide some indication of the operating condition of the instruments. Any stickiness of the rotor or vane, for example, will be evident. One such fault was detected, not in the field, but in the plot (Fig. 3): a sluggish vane at 4 m depth, whose variation is much less than that of the instruments above and below it. A fault like this would be obscured by any subsequent manipulation of the data to combine speed and direction or to incorporate them into other data. We show the 4 m data here for completeness, but we do not use them in later interpretation. Another error, a misalignment of the current meters at 30 and 40 m, was detected later by comparisons with auxiliary data from other current meters. The directions were corrected during data reduction. All of the other current meters appear to have produced satisfactory results.

Relative currents are useful for drag calculations where the velocity difference between ice and water is important. For other studies of ocean currents it is generally useful to remove the ice drift. In the extreme case when the ice is motionless, the relative observations are equivalent to true ocean currents. In the other extreme case of moving ice but motionless water, the relative currents reflect ice drift and the current meter acts as a pit log. In general, however, both ice and water are in motion, and true ocean currents are obtained by adding the ice velocity to the relative current velocity with due regard for their vectorial nature. In practice, the velocities are separated into their north and east components and the addition is performed separately on each component. Plots of true current speed and direction are shown in Figures 12-21. Progressive vector diagrams for the true currents are shown in Figures 22-31.

The current measurements for this study were made within two ranges of depth, each range characterized by a particular current behavior and physical regime. The first of these ranges, the planetary boundary layer, extends from the surface to a depth of about 35 m. (Salinity and temperature observations showed that the mixed layer also extended down to about 35 m during the observational period, so that these two layers can be considered here as essentially the same.) In the planetary boundary layer, currents move primarily under the influence of friction, horizontal pressure gradients, and the earth's rotation. There is a large shear in the upper part (5-10 m) of this layer during storms, but little shear occurs at any time in the lower part, where the flow is apparently nearly geostrophic. Since the water is also nearly homogeneous, it is essentially a barotropic flow.

The deep current measurements (at 40, 50, 70, and 100 m) were taken in the steep density gradient that extends downward from the planetary boundary layer to a depth of 300 m. In this region the currents also appear to be in nearly geostrophic equilibrium, but the flow is highly baroclinic, with strong vertical shears at all times. The swiftest currents appear at the deepest levels and are associated with baroclinic subsurface eddies. These eddies appear intermittently on the records, attaining speeds as great as 35 cm/sec at 100 m.

Means over periods longer than one hour are useful if currents are reasonably steady over the averaging interval chosen. The longer intervals tend to smooth out effects of turbulence and oscillating currents. A 12-hour interval was chosen to eliminate the effects of inertial and semidiurnal tidal motions, which both have periods close to 12 hours and which are noticeable in the ice velocity records and in some of the water velocity records. Both relative and absolute current means over 12-hour intervals are given at all ten depths in the Appendix. Mean ice velocity is also given.

ACKNOWLEDGMENT

These current experiments were made possible by the logistical support of the AIDJEX Office and the Naval Arctic Research Laboratory. Barry Allen and Allan Gill assisted with the measurements. The cooperation of all of the other investigators on the 1972 pilot study is gratefully acknowledged. This research was supported under contract N00014-67-A-0108-0016 with the Office of Naval Research.

REFERENCES

Hunkins, K. 1974. Subsurface eddies in the Arctic Ocean. *AIDJEX Bulletin No. 23*, 9-36.

Thorndike, A. 1973. An integrated system for measuring sea ice motions. In *Ocean 73, Proc. 1973 IEEE International Conference on Engineering in the Ocean Environment*. Institute of Electrical and Electronic Engineers, New York, N.Y., publ. 73 CH0774-0 OCC, pp. 490-499.

See also 1972 AIDJEX Pilot Study, *AIDJEX Bulletin No. 14*, July 1972.

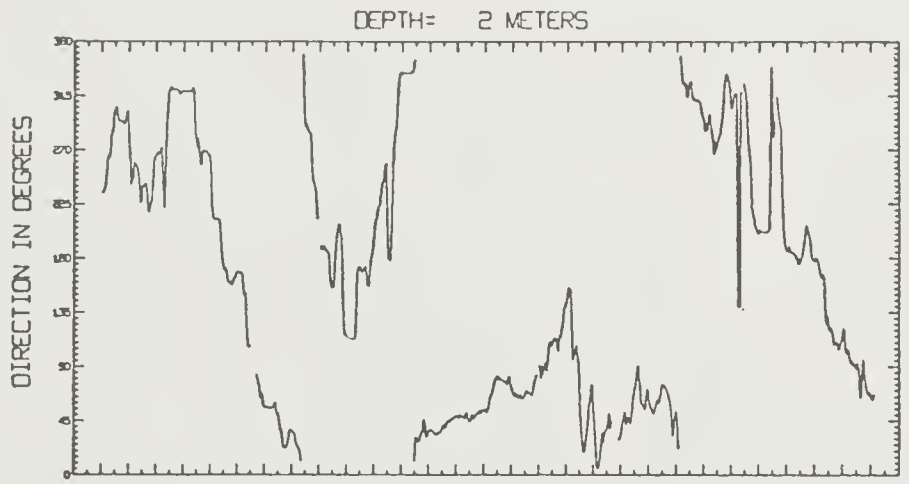

Fig. 2. Depth = 2 meters.

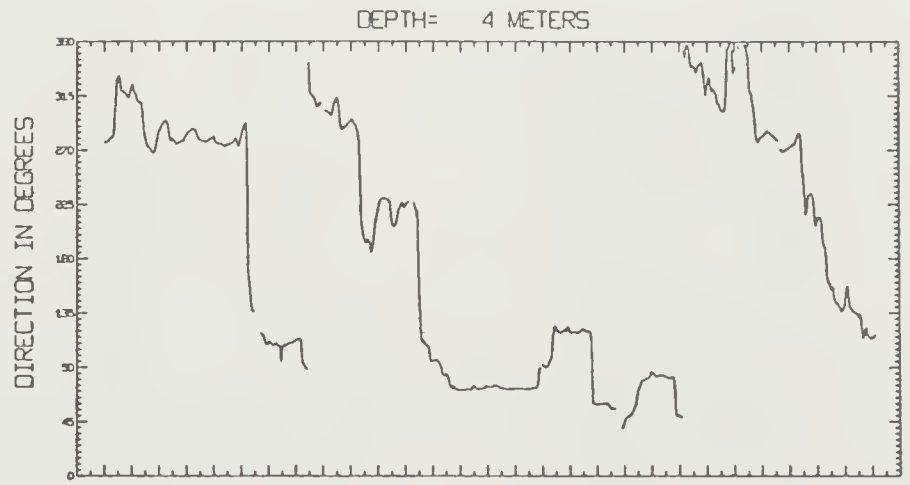

Fig. 3. Depth = 4 meters.

Figs. 2-11. Relative current speed and direction for specified depths below the base of the ice (sea level = 2 m), plotted at hourly intervals.

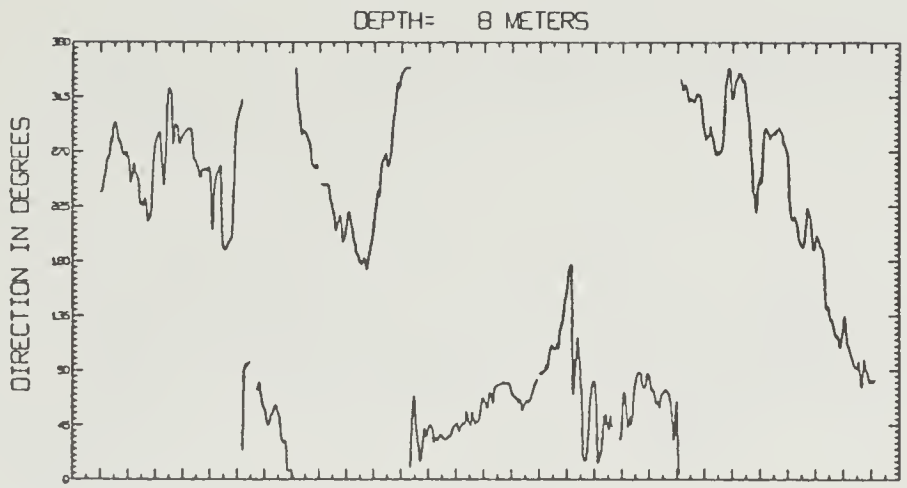

Fig. 4. Depth = 8 meters.

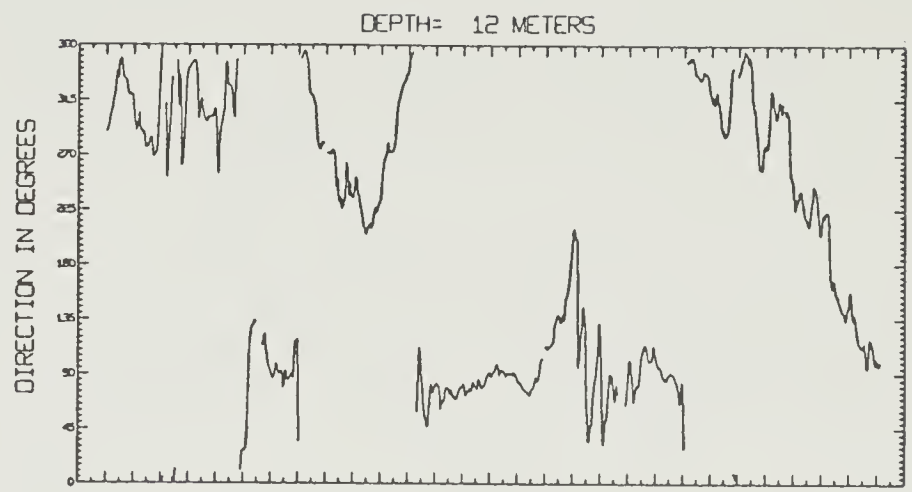

Fig. 5. Depth = 12 meters.

Figs. 2-11. Relative current speed and direction for specified depths below the base of the ice (sea level = 2 m), plotted at hourly intervals.

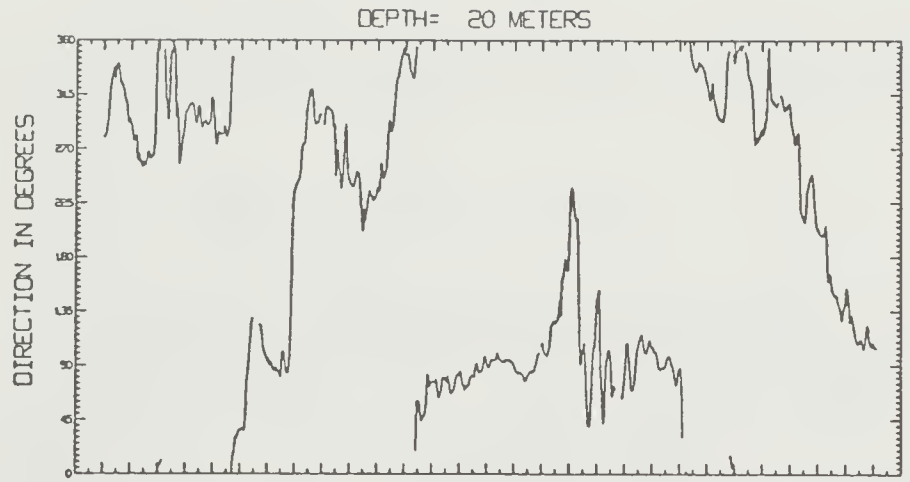

Fig. 6. Depth = 20 meters.

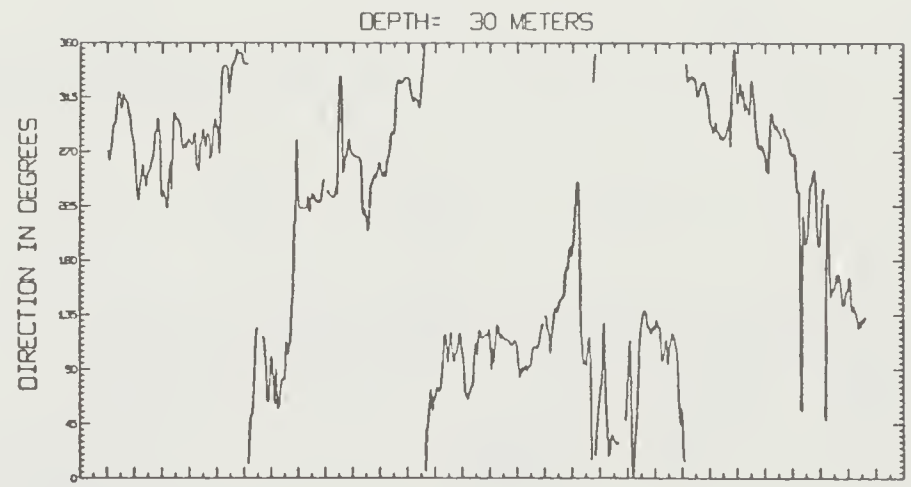

Fig. 7. Depth = 30 meters.

Figs. 2-11. Relative current speed and direction for specified depths below the base of the ice (sea level = 2 m), plotted at hourly intervals.

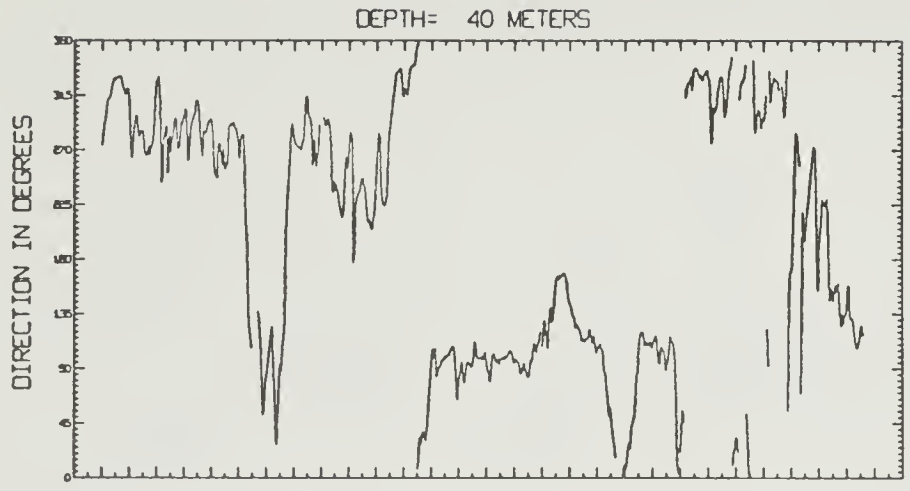

Fig. 8. Depth = 40 meters.

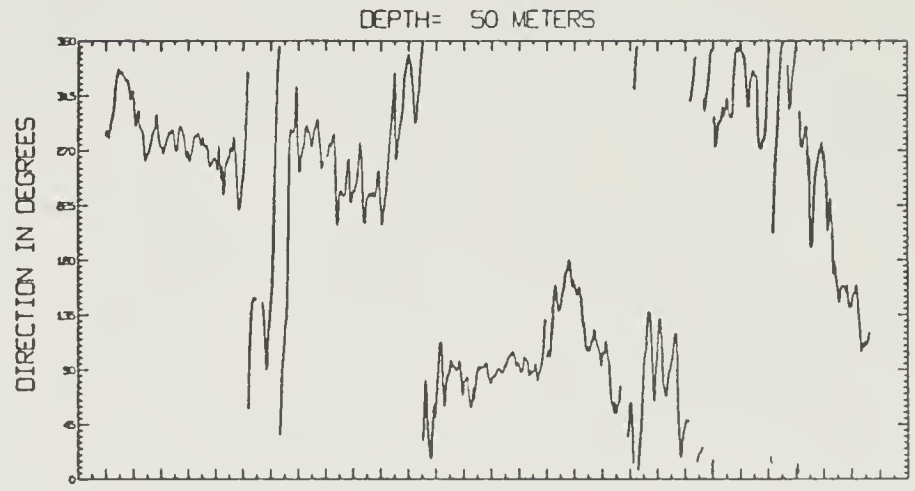

Fig. 9. Depth = 50 meters.

Figs. 2-11. Relative current speed and direction for specified depths below the base of the ice (sea level = 2 m), plotted at hourly intervals.

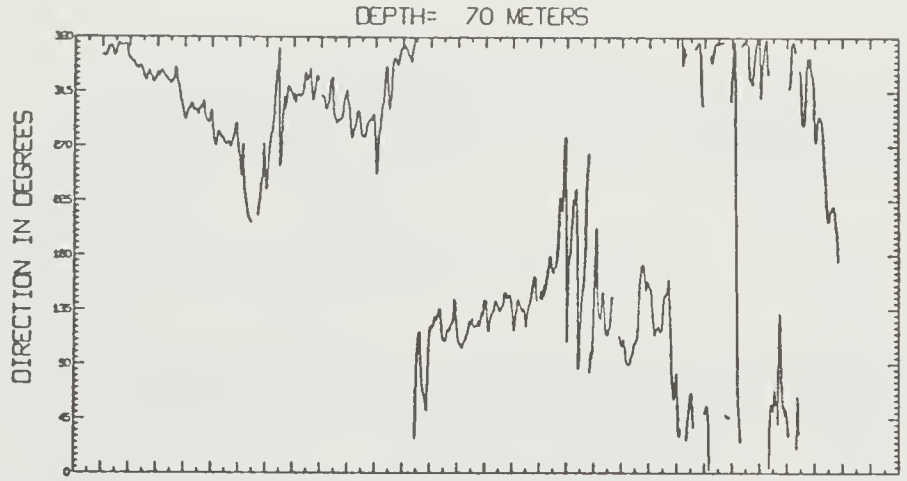

Fig. 10. Depth = 70 meters.

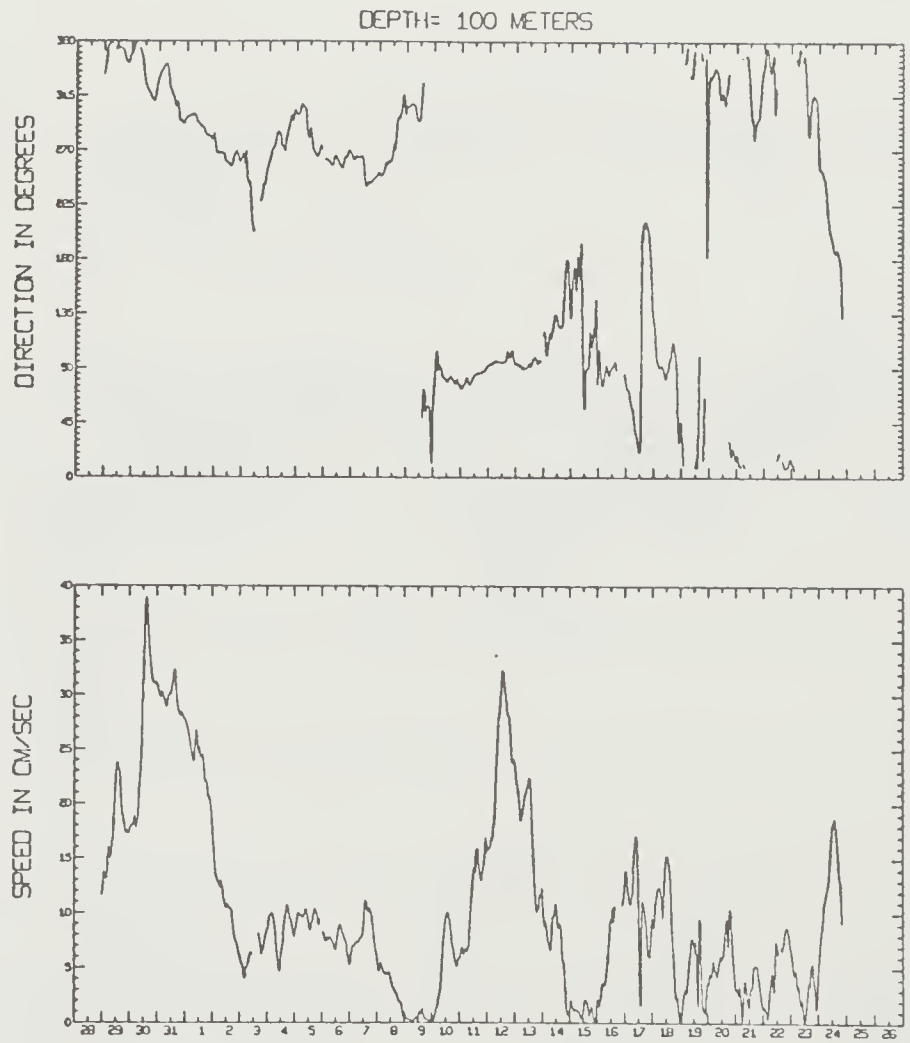

Fig. 11. Depth = 100 meters.

Figs. 2-11. Relative current speed and direction for specified depths below the base of the ice (sea level = 2 m), plotted at hourly intervals.

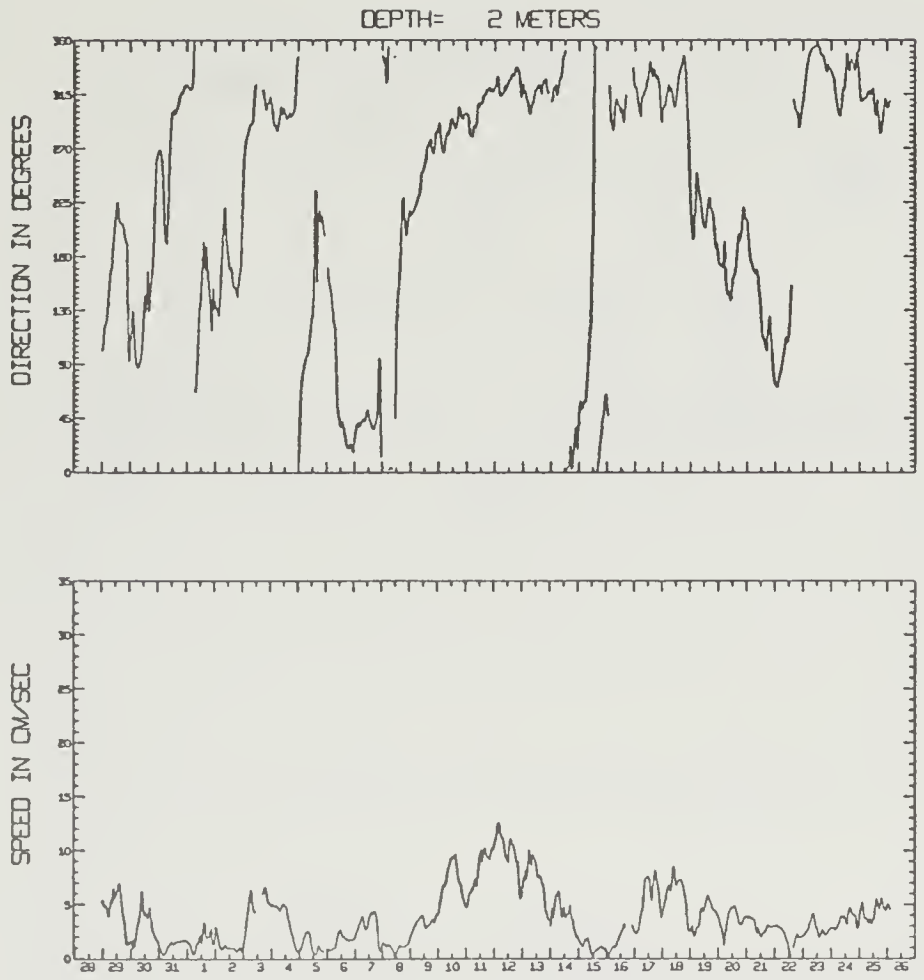

Fig. 12. Depth = 2 meters.

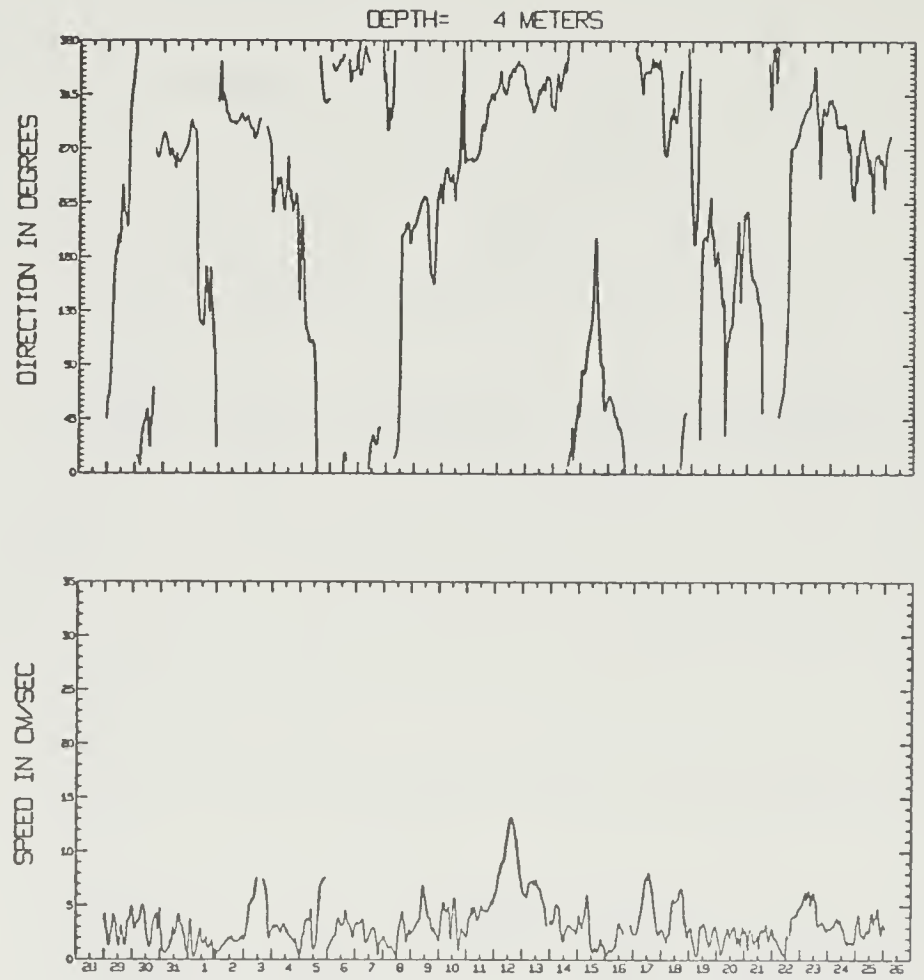

Fig. 13. Depth = 4 meters.

Figs. 12-21. True current speed and direction for specified depths below the base of the ice (sea level = 2 m), plotted at hourly intervals.

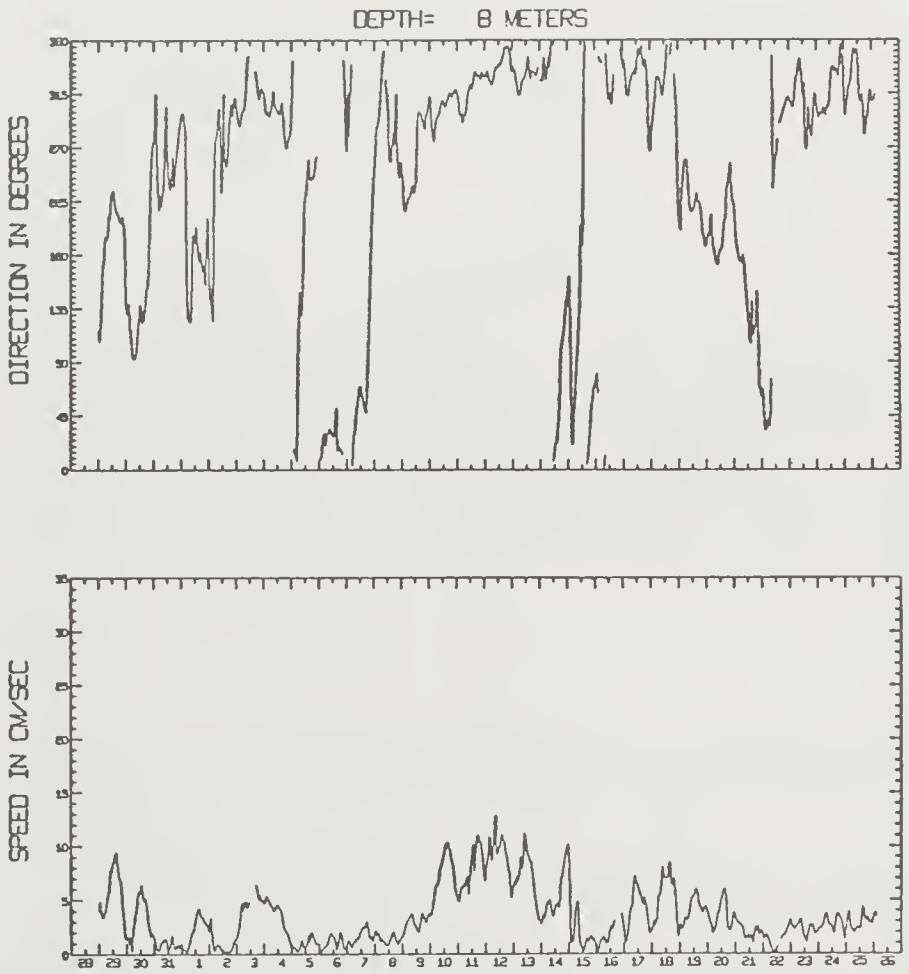

Fig. 14. Depth = 8 meters.

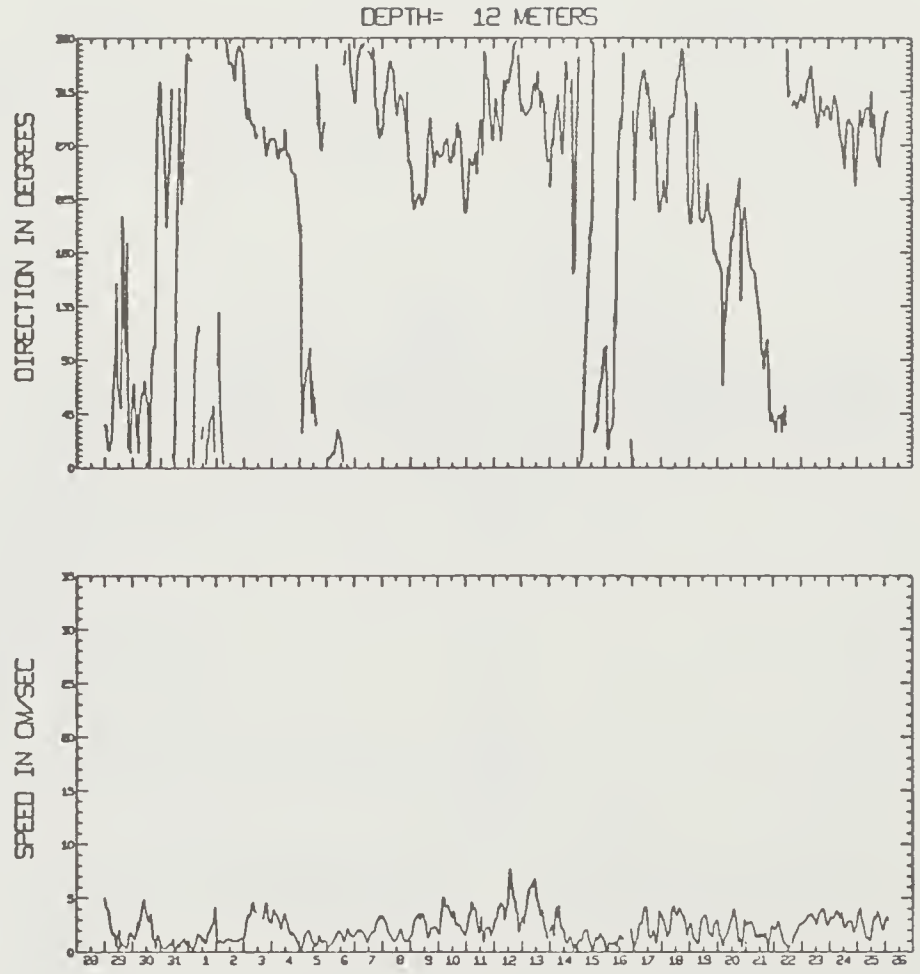

Fig. 15. Depth = 12 meters.

Figs. 12-21. True current speed and direction for specified depths below the base of the ice (sea level = 2 m), plotted at hourly intervals.

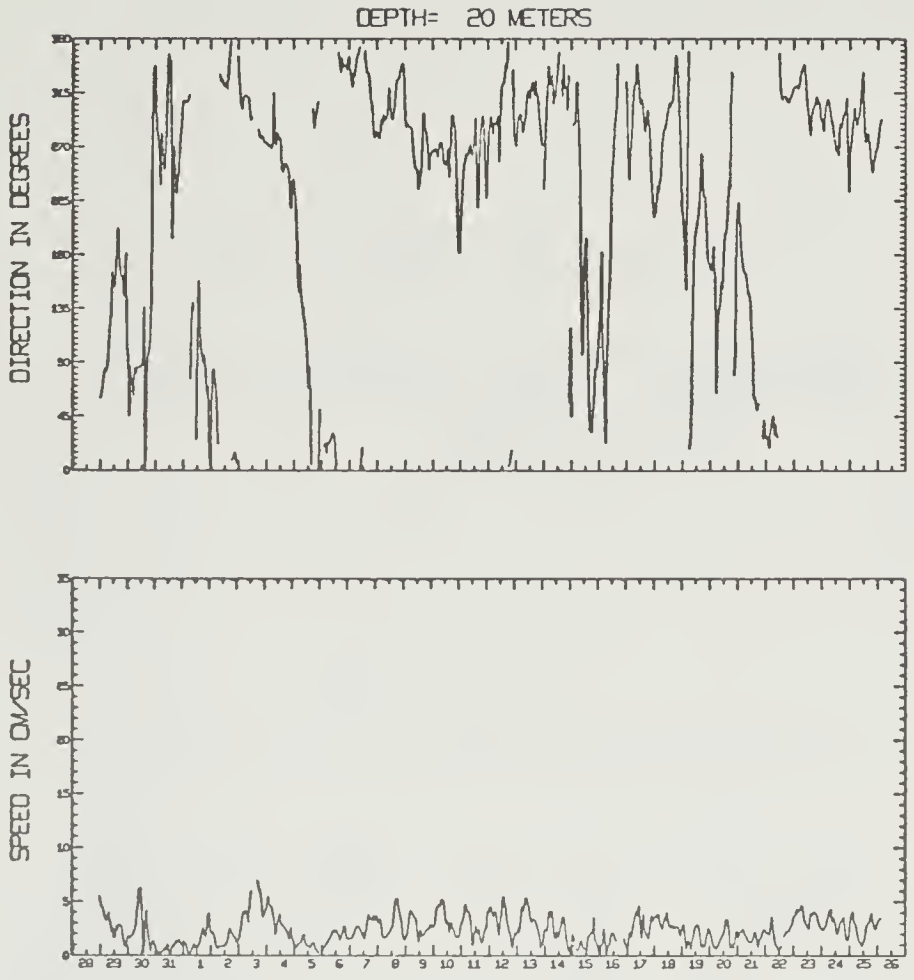

Fig. 16. Depth = 20 meters.

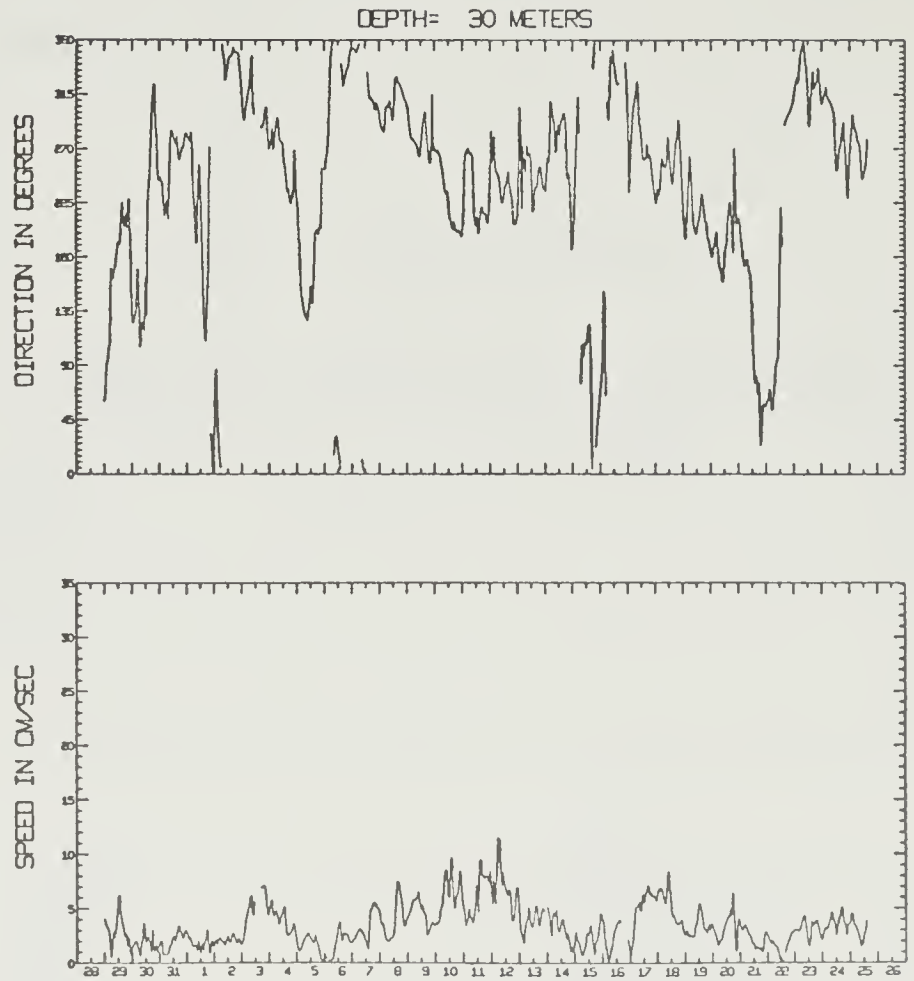

Fig. 17. Depth = 30 meters.

Figs. 12-21. True current speed and direction for specified depths below the base of the ice (sea level = 2 m), plotted at hourly intervals.

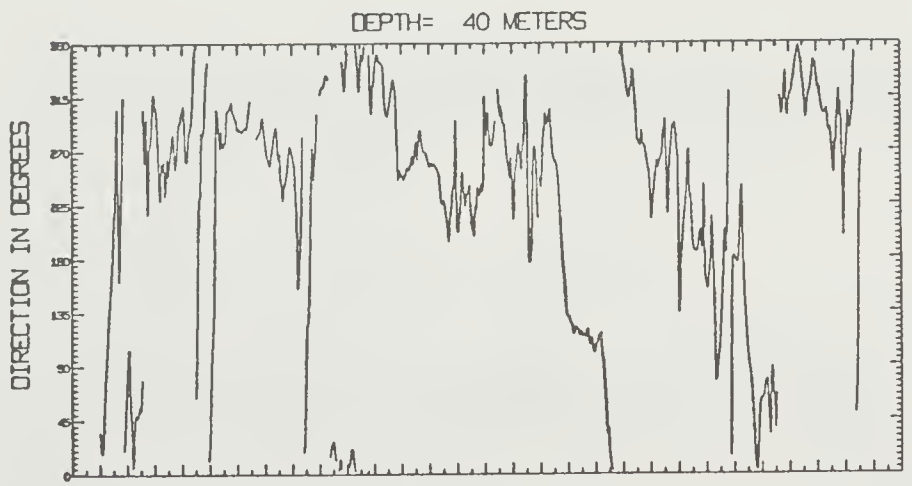

Fig. 18. Depth = 40 meters.

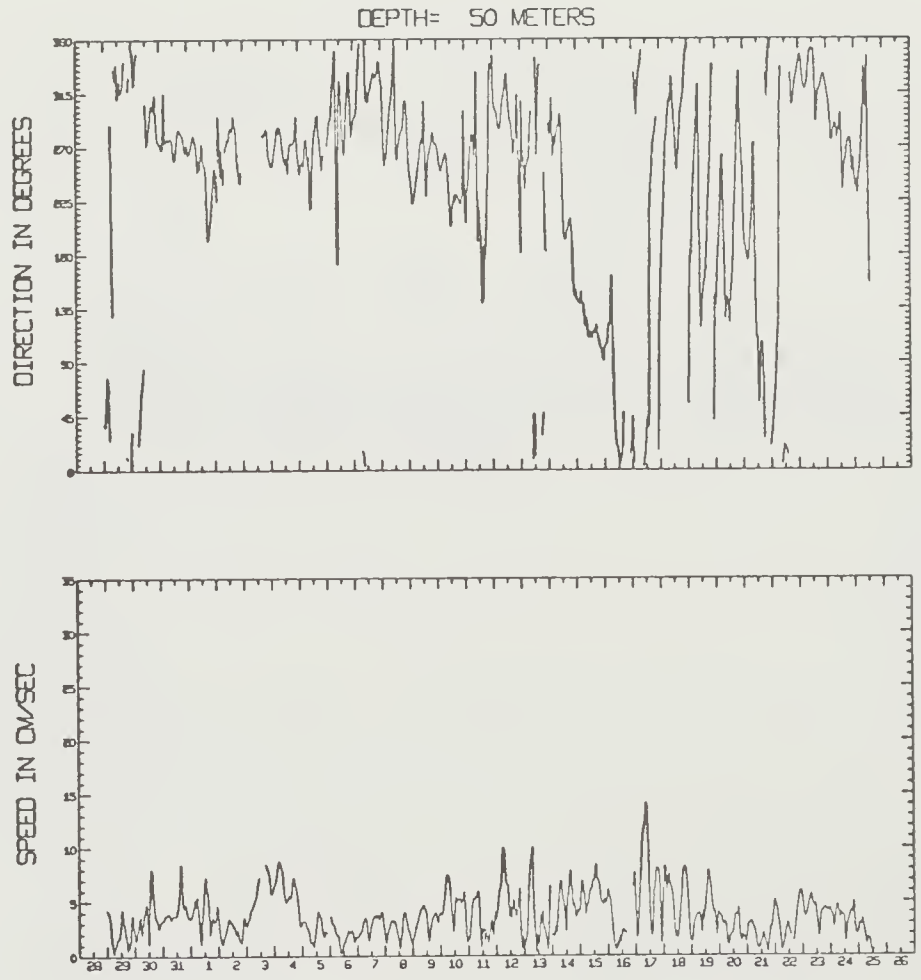

Fig. 19. Depth = 50 meters.

Figs. 12-21. True current speed and direction for specified depths below the base of the ice (sea level = 2 m), plotted at hourly intervals.

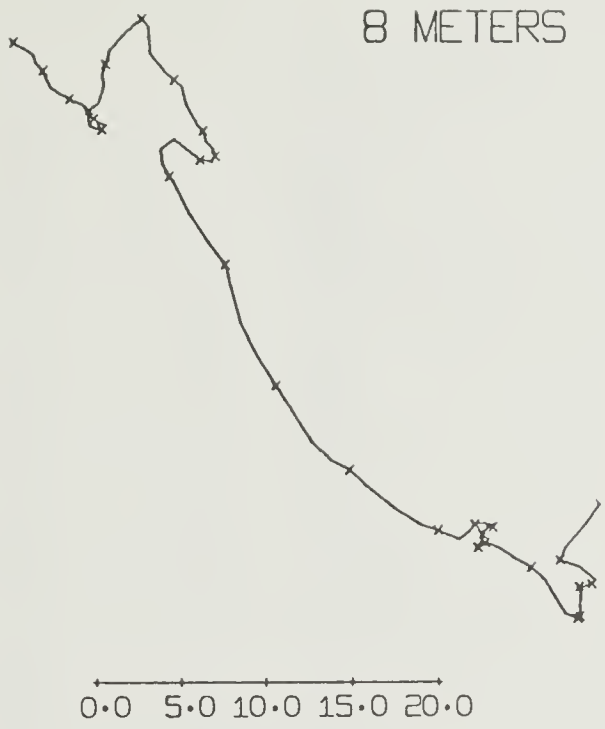

Fig. 24. Depth = 8 meters.

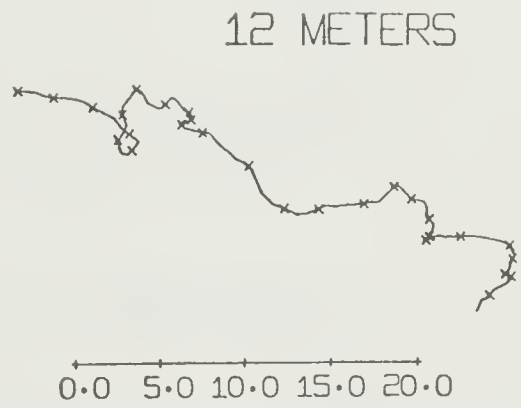

Fig. 25. Depth = 12 meters.

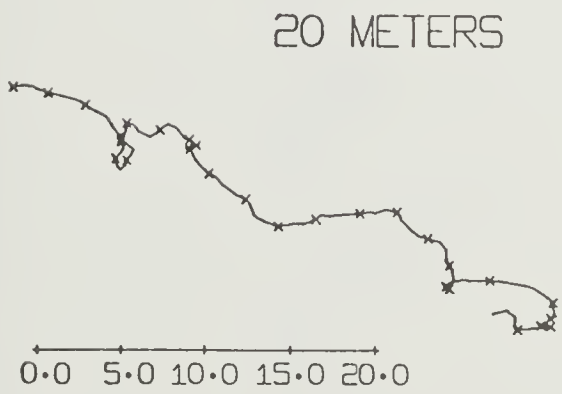

Fig. 26. Depth = 20 meters.

Figs. 22-31. Progressive vector diagrams for currents at specified depths below the base of the ice (sea level = 2 m), plotted at hourly intervals.

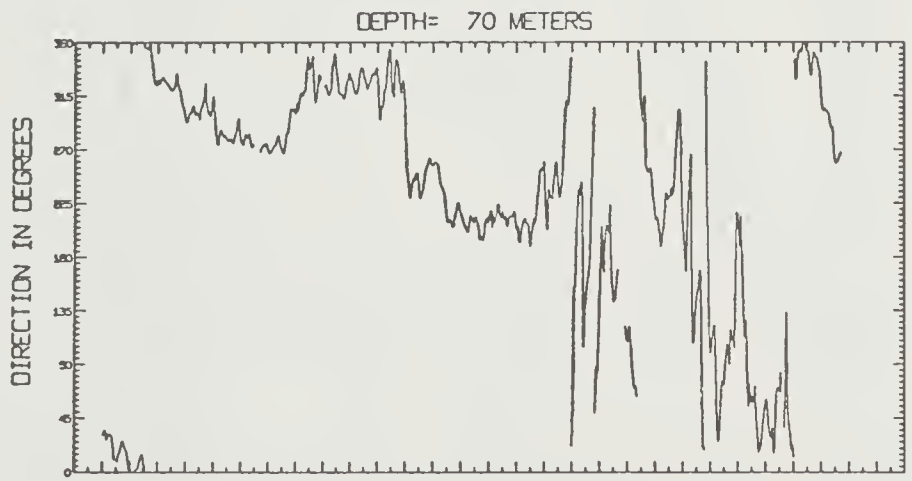

Fig. 20. Depth = 70 meters.

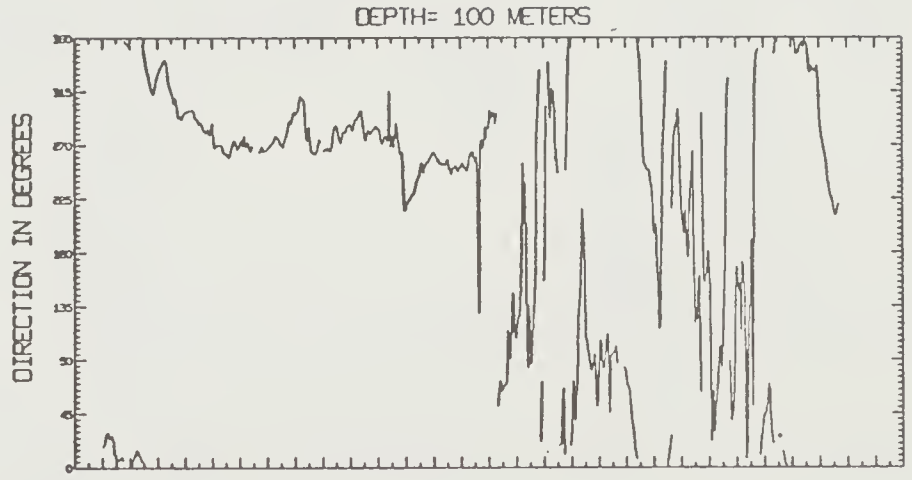

Fig. 21. Depth = 100 meters.

Figs. 12-21. True current speed and direction for specified depths below the base of the ice (sea level = 2 m), plotted at hourly intervals.

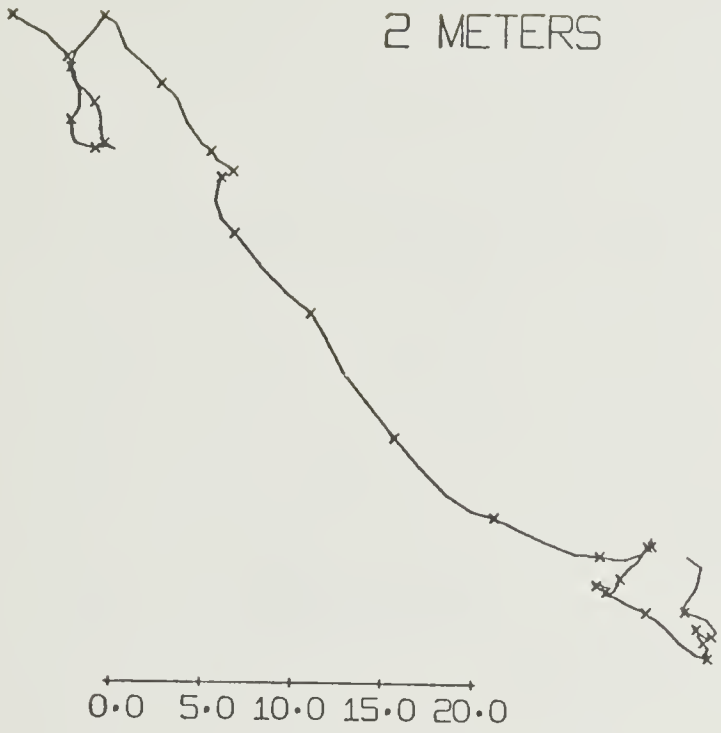

Fig. 22. Depth = 2 meters.

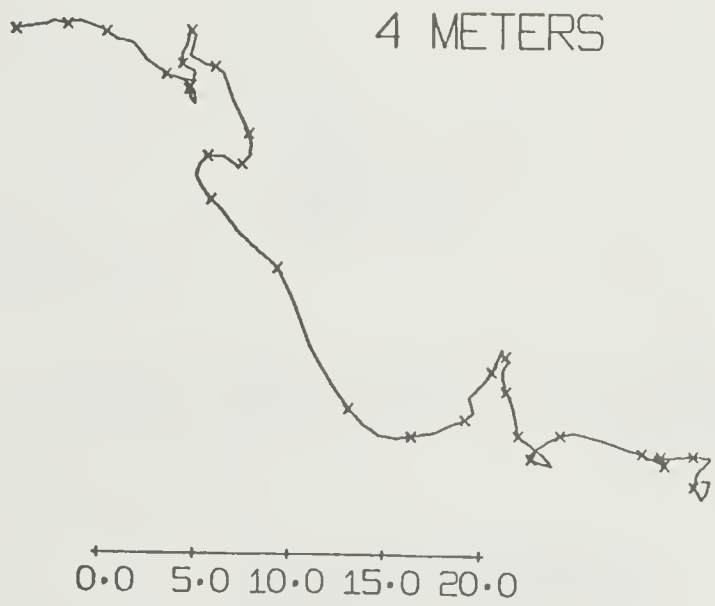

Fig. 23. Depth = 4 meters.

Figs. 22-31. Progressive vector diagrams for currents at specified depths below the base of the ice (sea level = 2 m), plotted at hourly intervals.

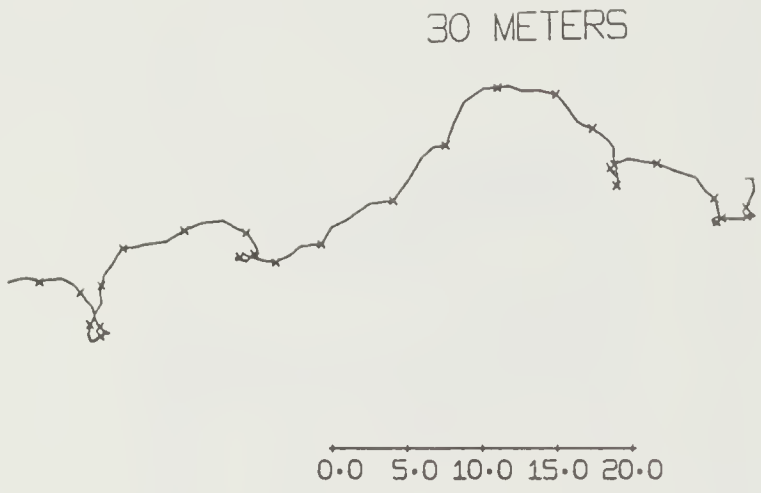

Fig. 27. Depth = 30 meters.

Fig. 28. Depth = 40 meters.

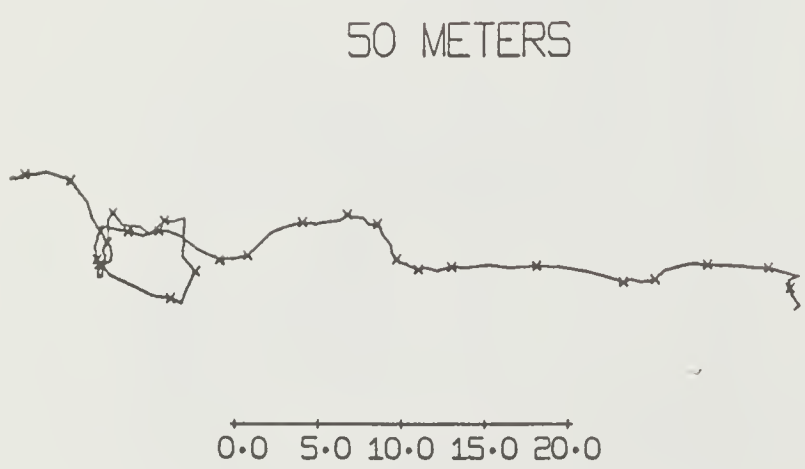

Fig. 29. Depth = 50 meters.

Figs. 22-31. Progressive vector diagrams for currents at specified depths below the base of the ice (sea level = 2 m), plotted at hourly intervals.

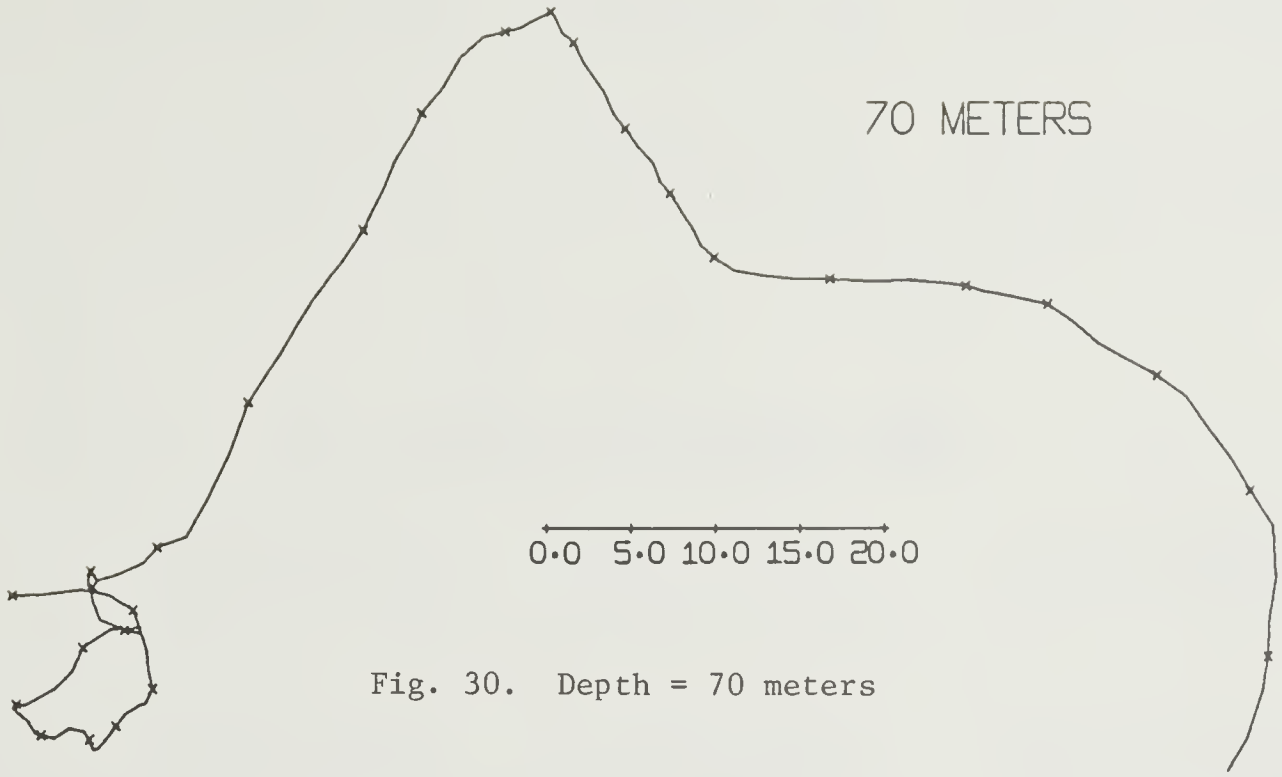

Fig. 30. Depth = 70 meters

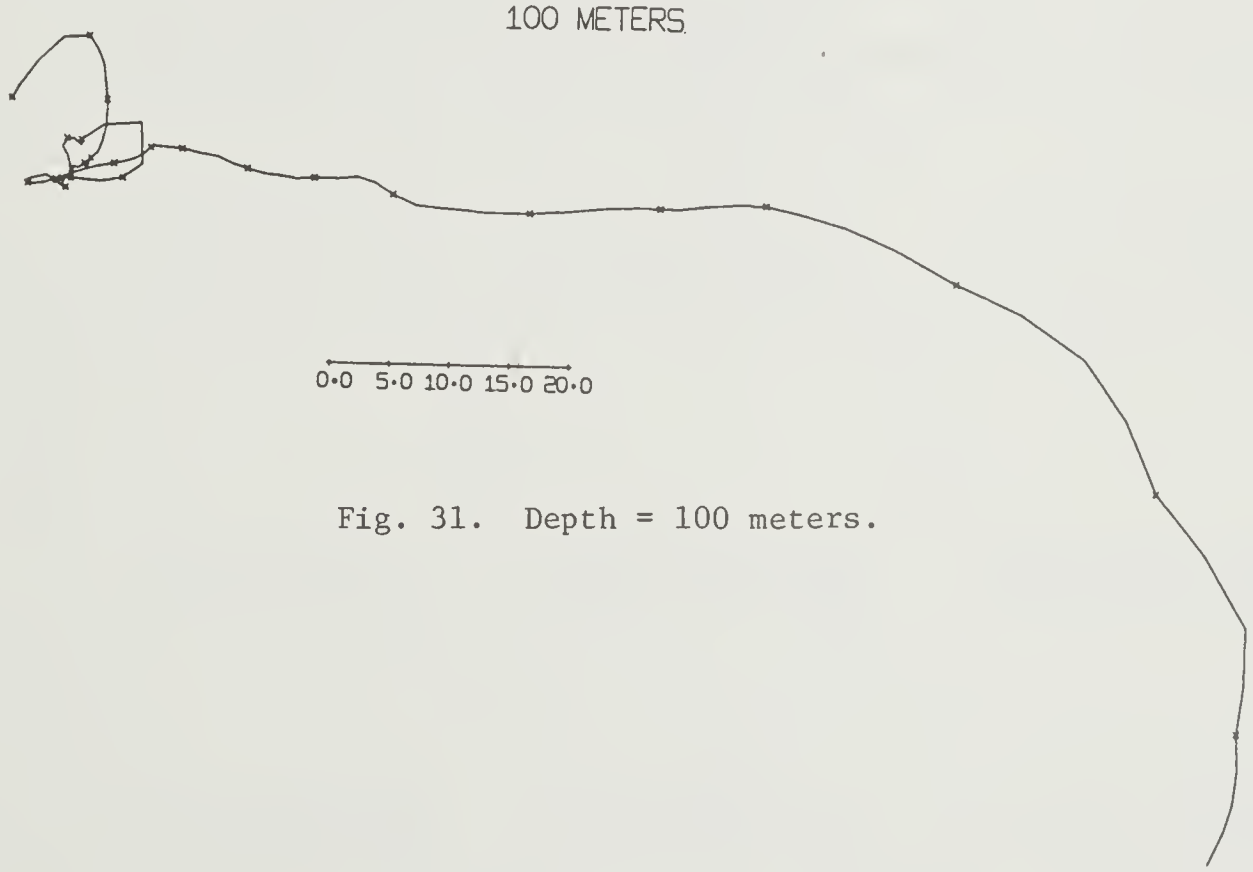

Fig. 31. Depth = 100 meters.

Figs. 22-31. Progressive vector diagrams for currents at specified depths below the base of the ice (sea level = 2 m), plotted at hourly intervals.

APPENDIX

CURRENT OBSERVATIONS AT THE MAIN CAMP
1972 AIDJEX PILOT STUDY

12-hour mean values
Velocity components in cm/sec
Time is Alaskan Standard Time
(AST = GMT - 10 hr).
Direction is given in terms of true north.

	Relative		Time	Absolute		Relative		Time	Absolute	
	V_E	V_N		V_E	V_N	V_E	V_N		V_E	V_N
29 Mar			0100-1200					1300-2400		
Ice				5.95	-3.85				4.10	-5.89
2 m	-4.62	-0.02		1.33	-3.88	-5.50	2.70		-1.39	-3.18
4	-5.34	2.40		0.60	-1.44	-5.61	6.66		-1.51	0.77
8	-6.90	-0.20		-0.95	-4.06	-7.58	1.09		-3.48	-4.79
12	-4.67	5.62		1.27	1.77	-3.63	6.34		0.46	0.45
20	-2.98	3.35		2.96	-0.50	-3.69	4.19		0.40	-1.69
30	-4.71	2.05		1.23	-1.80	-5.26	3.44		-1.15	-2.44
40	-4.39	3.78		1.55	-0.07	-4.21	5.98		-0.11	0.09
50	-5.35	4.92		0.59	1.06	-5.11	7.84		-1.01	1.95
70	-2.40	11.10		3.54	7.24	-2.02	14.21		2.06	8.31
100	-1.44	15.31		4.51	11.45	-3.63	19.54		0.46	13.65
30 Mar			0100-1200					1300-2400		
Ice				5.77	0.55				4.18	0.14
2 m	-2.97	-1.44		2.79	-0.89	-3.57	-2.36		0.60	-2.22
4	-3.90	2.66		1.86	3.22	-6.10	0.30		-1.92	0.44
8	-3.07	-1.68		2.68	-1.12	-2.68	-2.42		1.48	-2.28
12	-3.42	1.02		2.34	1.58	-3.59	0.76		0.58	0.91
20	-2.44	-0.18		3.32	0.36	-3.06	0.00		1.11	0.13
30	-4.38	-1.83		1.38	-1.27	-5.33	-0.29		-1.15	-0.14
40	-3.88	1.02		1.87	1.58	-5.51	0.37		-1.33	0.51
50	-4.69	1.07		1.08	1.62	-8.28	1.03		-4.10	1.17
70	-4.62	10.27		1.14	10.83	-7.62	11.71		-3.44	11.86
100	-4.21	19.80		1.55	20.36	-22.27	25.13		-18.08	25.27
31 Mar			0100-1200					1300-2400		
Ice				-0.11	-0.39				0.14	-0.42
2 m	-0.62	0.31		-0.74	-0.08	-1.28	1.49		-1.13	1.06
4	-1.33	0.34		-1.45	-0.04	-2.69	0.32		-2.54	-0.09
8	-0.63	0.19		-0.75	-0.20	-0.90	0.27		-0.76	-0.14
12	-0.18	0.55		-0.30	0.16	-0.62	0.63		-0.47	0.21
20	-0.26	0.55		-0.37	0.16	-1.00	0.37		-0.85	-0.04
30	-1.11	0.03		-1.22	-0.36	-2.83	0.61		-2.68	0.19
40	-1.03	0.13		-1.15	-0.25	-2.59	0.80		-2.44	0.38
50	-3.53	0.56		-3.65	0.17	-4.98	0.74		-4.83	0.32
70	-5.51	8.54		-5.63	8.14	-7.26	7.96		-7.11	7.54
100	-14.23	25.84		-14.34	25.44	-25.29	14.72		-25.14	14.29

	Relative		Time	Absolute		Relative		Time	Absolute	
	V_E	V_N		V_E	V_N	V_E	V_N		V_E	V_N
1 Apr			0100-1200					1300-2400		
Ice				1.44	-0.73				5.99	-1.46
2 m	-1.26	0.81		0.18	0.08	-5.27	-0.35		0.71	-1.81
4	-1.51	0.36		-0.06	-0.36	-5.36	0.79		0.61	-0.66
8	-1.36	0.10		0.08	-0.83	-6.07	-1.70		-0.08	-3.16
12	-1.01	1.05		0.42	0.32	-5.43	3.28		0.55	1.81
20	-1.61	0.98		-0.16	0.25	-4.54	2.22		1.44	0.76
30	-2.87	0.35		-1.42	-0.37	-5.35	1.21		0.63	-0.24
40	-2.26	1.24		-0.81	0.51	-7.34	1.97		-1.35	0.51
50	-5.39	0.51		-3.94	-0.21	-9.30	-0.30		-3.31	-1.76
70	-9.59	5.32		-8.14	4.59	-12.78	6.78		-6.78	5.32
100	-23.08	11.27		-21.63	10.54	-21.42	5.28		-15.42	3.82
2 Apr			0100-1200					1300-2400		
Ice				1.16	0.44				-0.24	0.61
2 m	-0.74	-1.59		0.40	-1.15	0.40	-1.39		0.16	-0.77
4	-2.30	0.20		-1.14	0.65	-1.48	0.16		-1.72	0.78
8	-1.04	-0.92		0.11	-0.48	-0.27	-0.32		-0.51	0.29
12	-1.02	0.32		0.12	0.76	-0.13	0.44		-0.37	1.06
20	-0.69	0.13		0.46	0.57	0.10	0.95		-0.13	1.57
30	-0.86	1.16		0.28	1.60	-0.28	1.41		-0.53	2.03
40	-1.90	-0.23		-0.75	0.20	-1.52	0.31		-1.77	0.92
50	-3.38	-0.78		-2.22	-0.34	-1.94	-0.65		-2.19	-0.03
70	-7.50	0.95		-6.34	1.39	-4.69	0.45		-4.93	1.07
100	-12.79	-0.80		-11.63	-0.36	-8.57	-1.23		-8.82	-0.61
3 Apr			0100-1200					1300-2400		
Ice				-4.97	2.28				-8.90	1.59
2 m	1.77	-0.85		-3.56	1.71	4.58	1.77		-4.43	3.65
4	0.73	-1.11		-4.61	1.45	4.86	-1.95		-4.15	-0.07
8	2.58	-0.10		-2.76	2.47	5.60	2.16		-3.41	4.03
12	2.14	-1.47		-3.19	1.09	5.63	-1.74		-3.38	0.12
20	2.36	-0.47		-2.97	2.10	4.11	-1.22		-4.90	0.64
30	2.40	0.41		-2.94	2.99	3.47	0.21		-5.54	2.09
40	0.89	-0.60		-4.45	1.96	2.51	0.18		-6.51	2.06
50	0.71	-1.19		-4.63	1.38	2.25	-1.37		-6.76	0.49
70	-1.51	-1.76		-6.87	0.80	-1.93	-1.47		-10.96	0.39
100	-4.13	-2.59		-9.49	-0.02	-6.60	-3.11		-15.63	-1.23

	Relative		Time	Absolute		Relative		Time	Absolute	
	V_E	V_N		V_E	V_N	V_E	V_N		V_E	V_N
4 Apr			0100-1200					1300-2400		
Ice				-7.34	0.00				-3.15	-0.53
2 m	2.97	2.06		-4.36	2.06	1.12	1.75		-2.02	1.22
4	4.80	-1.53		-2.53	-1.53	2.30	-0.78		-0.84	-1.31
8	3.46	2.49		-3.87	2.49	0.95	1.42		-2.19	0.89
12	4.18	0.04		-3.14	0.04	1.66	-0.03		-1.47	-0.56
20	3.46	0.19		-3.86	0.19	1.13	-0.40		-2.01	-0.93
30	2.87	0.75		-4.46	0.76	0.45	-0.82		-2.69	-1.35
40	2.22	0.27		-5.11	0.27	-0.32	-0.55		-3.47	-1.08
50	0.60	0.17		-6.73	0.17	-1.92	0.32		-5.07	-0.20
70	-1.89	0.55		-9.24	0.55	-3.48	2.91		-6.64	2.38
100	-7.72	0.65		-15.07	0.65	-8.21	3.03		-11.36	2.50
5 Apr			0100-1200					1300-2400		
Ice				1.60	-0.94				1.12	-0.47
2 m	-0.02	0.70		1.58	-0.23	-1.33	-0.17		-0.28	-0.58
4	0.80	0.10		2.41	-0.84	-4.58	3.77		-3.53	3.35
8	-1.39	0.84		0.20	-0.09	-2.28	-0.07		-1.23	-0.48
12	-0.46	1.14		1.13	0.19	-1.72	0.66		-0.67	0.25
20	-0.90	0.24		0.69	-0.70	-1.27	0.78		-0.23	0.36
30	-0.55	-0.52		1.03	-1.47	-1.08	-0.88		-0.04	-1.30
40	-1.96	0.64		-0.36	-0.29	-1.92	0.19		-0.87	-0.21
50	-3.59	0.36		-1.99	-0.57	-3.81	0.77		-2.76	0.36
70	-4.53	4.79		-2.92	3.84	-4.12	5.15		-3.07	4.74
100	-8.48	4.31		-6.87	3.37	-9.32	0.07		-8.27	-0.33
6 Apr			0100-1200					1300-2400		
Ice				1.04	1.35				0.84	2.24
2 m	-0.06	-1.13		0.91	0.14	0.04	-0.55		0.89	1.68
4	-1.51	1.06		-0.52	2.33	-1.85	0.68		-1.00	2.93
8	-0.45	-0.31		0.52	0.94	-0.70	-1.39		0.14	0.83
12	-0.52	-0.12		0.45	1.15	-1.26	-0.85		-0.41	1.37
20	-0.37	0.11		0.61	1.38	-1.46	-0.35		-0.61	1.87
30	-0.75	-0.43		0.23	0.83	-1.46	0.08		-0.62	2.32
40	-1.41	0.28		-0.42	1.55	-1.05	-0.68		-0.20	1.54
50	-2.43	-0.56		-1.44	0.70	-2.41	-1.54		-1.56	0.68
70	-3.27	2.74		-2.28	4.01	-4.65	2.42		-3.80	4.66
100	-7.40	-1.11		-6.41	0.16	-7.43	-1.01		-6.58	1.21

	Relative		Time	Absolute		Relative		Time	Absolute	
	V_E	V_N		V_E	V_N	V_E	V_N		V_E	V_N
7 Apr			0100-1200					1300-2400		
Ice				1.22	3.42				1.54	5.18
2 m	0.83	-1.22		2.05	2.19	0.34	-3.04		1.88	2.12
4	-1.63	-0.73		-0.41	2.68	-1.22	-3.47		0.30	1.69
8	-0.76	-2.72		0.45	0.69	-0.60	-4.98		0.93	0.19
12	-1.59	-1.87		-0.37	1.54	-3.43	-3.99		-1.89	1.18
20	-1.69	-1.35		-0.47	2.06	-3.95	-3.59		-2.41	1.58
30	-1.29	-0.86		-0.07	2.54	-4.81	-2.42		-3.27	2.75
40	-1.46	-0.78		-0.24	2.63	-2.26	-2.68		-0.72	2.48
50	-1.99	-1.44		-0.77	1.97	-3.41	-2.35		-1.87	2.82
70	-4.15	1.41		-2.92	4.84	-5.62	1.59		-4.08	6.77
100	-7.08	-1.19		-5.85	2.22	-8.34	-3.84		-6.80	1.33
8 Apr			0100-1200					1300-2400		
Ice				0.30	1.42				-0.02	-1.01
2 m	-0.43	-0.51		-0.13	0.89	-0.39	-0.02		-0.42	-1.03
4	-0.75	-0.67		-0.45	0.73	-1.08	-1.63		-1.11	-2.65
8	-1.26	-0.77		-0.96	0.63	-1.42	0.83		-1.44	-0.17
12	-1.43	-0.09		-1.13	1.32	-1.22	1.52		-1.25	0.50
20	-2.40	-0.47		-2.10	0.93	-2.02	3.66		-2.05	2.64
30	-2.71	-0.29		-2.41	1.11	-3.20	4.98		-3.23	3.96
40	-1.02	-0.09		-0.71	1.32	-1.74	2.18		-1.76	1.16
50	-2.28	-0.57		-1.97	0.84	-2.14	1.52		-2.17	0.50
70	-2.44	0.99		-2.13	2.41	-1.02	2.74		-1.05	1.72
100	-4.56	-1.08		-4.25	0.32	-1.90	0.77		-1.92	-0.23
9 Apr			0100-1200					1300-2400		
Ice				-2.53	-2.32				-4.48	-1.32
2 m	-0.14	0.51		-2.67	-1.80	1.11	1.70		-3.36	0.37
4	-0.14	-0.79		-2.67	-3.11	4.01	-1.39		-0.46	-2.72
8	0.33	0.38		-2.18	-1.92	1.73	2.66		-2.74	1.33
12	0.45	0.17		-2.07	-2.14	2.54	1.10		-1.93	-0.22
20	-0.30	2.22		-2.83	-0.10	2.20	1.26		-2.27	-0.06
30	-2.82	2.94		-5.35	0.61	0.86	1.85		-3.61	0.52
40	-0.63	1.60		-3.16	-0.71	1.14	1.33		-3.33	0.00
50	-0.65	1.22		-3.18	-1.09	1.46	1.32		-3.01	0.00
70	-0.02	1.00		-2.55	-1.31	0.82	0.00		-3.65	-1.32
100	-0.29	0.18		-2.82	-2.13	0.24	0.32		-4.23	-0.99

	Relative		Time	Absolute		Relative		Time	Absolute	
	V_E	V_N		V_E	V_N	V_E	V_N		V_E	V_N
10 Apr			0100-1200					1300-2400		
Ice				-9.48	-1.82				-12.46	-3.12
2 m	2.44	3.42		-7.03	1.59	6.03	6.15		-6.42	3.03
4	5.90	0.24		-3.57	-1.57	9.55	2.63		-2.90	-0.47
8	3.56	4.87		-5.90	3.05	6.44	8.49		-6.01	5.36
12	5.71	1.48		-3.76	-0.33	10.26	2.82		-2.19	-0.29
20	5.36	1.40		-4.11	-0.41	10.63	2.73		-1.81	-0.38
30	4.28	-0.39		-5.18	-2.21	9.70	-3.21		-2.75	-6.33
40	3.73	-0.46		-5.74	-2.29	8.73	-0.88		-3.72	-4.00
50	4.87	0.34		-4.60	-1.46	9.41	0.18		-3.04	-2.93
70	3.20	-1.71		-6.27	-3.53	7.32	-4.22		-5.13	-7.35
100	3.61	0.41		-5.86	-1.40	7.27	1.27		-5.18	-1.84
11 Apr			0100-1200					1300-2400		
Ice				-12.14	-2.54				-15.91	-0.53
2 m	5.92	5.36		-6.20	2.82	9.21	7.67		-6.68	7.13
4	8.20	2.62		-3.93	0.09	12.23	3.75		-3.67	3.21
8	6.88	6.47		-5.25	3.93	11.19	8.35		-4.70	7.81
12	9.13	1.78		-2.99	-0.75	14.26	1.41		-1.63	0.87
20	9.05	1.96		-3.08	-0.56	13.86	0.17		-2.03	-0.36
30	8.39	0.61		-3.73	-1.91	11.52	-5.80		-4.38	-6.33
40	8.85	-0.06		-3.27	-2.59	12.69	-2.47		-3.21	-3.01
50	8.69	2.06		-3.43	-0.47	15.36	0.40		-0.54	-0.13
70	8.55	-3.80		-3.57	-6.34	11.45	-8.90		-4.45	-9.44
100	7.95	1.49		-4.17	-1.04	14.68	0.56		-1.22	0.02
12 Apr			0100-1200					1300-2400		
Ice				-20.45	2.85				-22.69	3.73
2 m	13.57	5.51		-6.86	8.36	18.28	3.81		-4.40	7.54
4	15.67	4.51		-4.77	7.36	18.54	5.90		-4.14	9.64
8	15.68	5.80		-4.76	8.65	20.71	4.31		-1.97	8.05
12	17.39	-0.80		-3.05	2.03	20.96	0.14		-1.73	3.87
20	17.21	-1.46		-3.22	1.37	21.57	-1.34		-1.11	2.38
30	13.45	-5.65		-6.98	-2.80	18.57	-7.52		-4.11	-3.78
40	14.63	-1.02		-5.81	1.81	17.88	-3.01		-4.80	0.71
50	15.05	0.34		-5.38	3.18	19.63	-2.92		-3.05	0.80
70	13.41	-12.57		-7.02	-9.72	14.05	-17.54		-8.63	-13.81
100	20.87	-1.81		0.43	1.02	27.64	-4.07		4.94	-0.34

	Relative		Time	Absolute		Relative		Time	Absolute	
	V_E	V_N		V_E	V_N	V_E	V_N		V_E	V_N
13 Apr			0100-1200					1300-2400		
Ice				-19.80	-0.30				-14.30	1.40
2 m	13.36	5.92		- 6.43	5.62	9.69	3.07		-3.73	4.57
4	14.74	4.70		- 5.05	4.39	10.20	2.52		-3.22	4.02
8	15.03	7.26		- 4.76	6.96	10.86	3.88		-2.56	5.38
12	15.71	3.36		- 4.07	3.06	11.18	0.17		-2.23	1.66
20	16.59	2.24		- 3.20	1.93	11.58	0.06		-1.84	1.56
30	16.56	-0.05		- 3.23	-0.36	9.58	-3.91		-3.84	-2.41
40	15.01	-0.07		- 4.77	-0.37	11.15	-2.51		-2.26	-1.01
50	16.39	-0.05		- 3.40	-0.35	12.54	-1.17		-0.87	0.32
70	14.23	-12.72		- 5.55	-13.02	6.59	-8.64		-6.83	-7.14
100	20.72	-0.64		- 0.92	-0.95	14.50	-1.85		1.06	-0.36
14 Apr			0100-1200					1300-2400		
Ice				-8.45	4.71				-3.31	5.02
2 m	5.89	-0.70		-2.55	4.00	4.07	-1.87		0.76	3.14
4	6.61	-1.71		-1.83	2.99	4.72	-2.71		1.41	2.30
8	7.35	-0.98		-1.09	3.72	8.55	-6.55		5.24	-1.53
12	5.95	-3.99		-2.49	0.71	2.96	-4.60		-0.34	0.42
20	6.64	-2.77		-1.80	1.93	2.45	-3.57		-0.85	1.44
30	4.85	-4.03		-3.59	0.67	1.36	-4.90		-1.93	0.12
40	3.87	-3.66		-4.57	1.05	3.11	-9.04		-0.19	-4.01
50	4.73	-3.86		-3.71	0.84	2.76	-9.72		-0.54	-4.69
70	3.05	-8.34		-5.39	-3.62	-0.41	-4.61		-3.72	0.41
100	7.48	-4.34		-0.96	0.36	3.60	-3.52		0.29	1.49
15 Apr			0100-1200					1300-2400		
Ice				-0.01	0.85				0.00	0.18
2 m	1.08	-0.60		1.06	0.24	0.38	0.46		0.38	0.65
4	3.33	-1.85		3.31	-1.00	0.82	-0.10		0.83	0.08
8	1.63	-1.12		1.62	-0.26	0.52	0.58		0.53	0.77
12	0.60	-0.75		0.58	0.09	0.82	0.28		0.82	0.46
20	-0.30	-0.83		-0.32	0.01	1.21	0.34		1.21	0.53
30	0.30	-1.30		0.28	-0.45	1.94	0.79		1.95	0.97
40	9.68	-6.79		9.66	-5.94	8.65	-3.66		8.65	-3.47
50	4.49	-4.32		4.47	-3.47	5.69	-2.00		5.69	-1.81
70	-0.28	-2.00		-0.30	-1.15	0.64	-1.26		0.64	-1.08
100	0.37	-0.86		0.35	0.00	1.16	-0.12		1.17	0.06

	Relative		Time	Absolute		Relative		Time	Absolute	
	V_E	V_N		V_E	V_N	V_E	V_N		V_E	V_N
16 Apr			0100-1200					1300-2400		
Ice				-1.48	-0.41				-3.42	-0.01
2 m	0.56	1.02		-0.90	0.60	1.36	1.78		-2.02	1.81
4	2.37	1.44		0.89	1.02	3.30	2.68		-0.09	2.72
8	1.11	1.43		-0.36	1.01	2.00	2.32		-1.38	2.36
12	1.54	0.55		0.06	0.14	2.87	0.83		-0.51	0.87
20	1.56	0.30		0.08	-0.10	2.40	0.89		-0.98	0.93
30	1.77	1.42		0.29	1.00	1.88	2.31		-1.50	2.35
40	5.41	0.46		3.93	0.05	2.89	9.20		-0.50	9.24
50	3.27	0.28		1.79	-0.13	4.95	3.53		1.55	3.57
70	1.47	-1.33		0.00	-1.75	7.45	-4.33		4.05	-4.30
100	4.32	0.17		2.84	-0.23	10.46	0.38		7.06	0.42
17 Apr			0100-1200					1300-2400		
Ice				-5.84	1.72				-10.71	2.34
2 m	2.66	1.92		-3.16	3.64	7.35	2.61		- 3.34	4.96
4	3.78	2.46		-2.05	4.18	8.65	1.59		- 2.05	3.94
8	3.68	1.99		-2.15	3.71	9.24	1.03		- 1.46	3.38
12	4.16	0.06		-1.67	1.78	9.19	-2.87		- 1.50	-0.53
20	3.89	-0.02		-1.93	1.69	8.54	-2.75		- 2.15	-0.41
30	2.16	0.18		-3.66	1.89	4.76	-3.87		- 5.93	-1.52
40	3.02	2.30		-2.80	4.02	5.73	-2.55		- 4.96	-0.21
50	4.31	5.59		-1.52	7.31	7.97	-2.66		- 2.73	-0.31
70	8.04	-1.27		2.20	0.44	2.82	-5.16		- 7.88	-2.81
100	9.34	8.83		3.50	10.55	-0.82	-5.85		-11.53	-3.50
18 Apr			0100-1200					1300-2400		
Ice				-12.27	0.19				- 8.68	1.38
2 m	7.44	4.20		-4.81	4.39	5.95	2.64		- 2.71	4.03
4	9.23	1.07		-3.03	1.26	8.87	1.69		0.20	3.08
8	8.94	3.56		-3.31	3.75	7.79	3.32		- 0.88	4.71
12	9.83	-0.02		-2.43	0.16	7.13	0.55		- 1.53	1.94
20	9.32	-0.37		-2.93	0.18	6.99	-0.25		- 1.67	1.13
30	6.19	-2.35		-6.06	-2.16	5.24	-1.99		- 3.43	-0.60
40	6.59	-1.52		-5.66	-1.33	5.73	-1.06		- 2.93	0.32
50	8.78	-0.98		-3.47	-0.79	4.96	0.51		- 3.70	1.90
70	8.45	-5.91		-3.80	-5.72	3.38	-3.44		- 5.28	-2.05
100	11.27	-0.49		-0.99	-0.30	6.84	-0.80		- 1.83	0.58

	Relative		Time	Absolute		Relative		Time	Absolute	
	V_E	V_N		V_E	V_N	V_E	V_N		V_E	V_N
19 Apr			0100-1200					1300-2400		
Ice				0.14	-5.56				1.95	-7.71
2 m	-2.02	2.97		-1.87	-2.57	-4.12	3.57		-2.16	-4.12
4	-0.76	3.85		-0.61	-1.70	-2.41	5.39		-0.46	-2.31
8	-2.78	3.34		-2.62	-2.21	-4.43	3.84		-2.48	-3.86
12	-1.22	4.22		-1.07	-1.33	-2.79	5.53		-0.84	-2.16
20	-0.23	4.53		-0.08	-1.02	-2.66	6.26		-0.71	-1.44
30	-1.77	3.10		-1.62	-2.45	-3.72	4.49		-1.76	-3.21
40	-1.80	3.54		-1.64	-2.01	-2.37	4.57		-0.42	-3.13
50	-0.84	4.29		-0.69	-1.26	-2.11	4.82		-0.16	-2.88
70	1.55	3.18		1.70	-2.37	-0.30	5.91		1.64	-1.79
100	-1.01	3.96		-0.86	-1.58	-0.06	3.40		1.89	-4.30
20 Apr			0100-1200					1300-2400		
Ice				3.97	-3.67				1.67	-5.45
2 m	-2.80	0.63		1.15	-3.02	-2.58	1.84		-0.90	-3.60
4	-2.62	2.70		1.33	-0.95	-2.21	3.31		-0.53	-2.13
8	-4.28	0.49		-0.31	-3.17	-3.68	2.33		-2.00	-3.11
12	-3.45	2.13		0.50	-1.52	-2.75	3.56		-1.07	-1.88
20	-3.62	2.56		0.33	-1.10	-2.67	4.25		-0.99	-1.19
30	-3.87	1.05		0.08	-2.61	-3.51	2.20		-1.83	-3.24
40	-2.56	2.43		1.39	-1.23	-1.63	3.76		0.04	-1.68
50	-4.11	1.95		-0.15	-1.70	-2.63	4.22		-0.95	-1.22
70	-0.07	4.59		3.89	0.92	1.11	3.93		2.79	-1.51
100	-2.61	4.03		1.34	0.36	-0.59	6.21		1.08	0.76
21 Apr			0100-1200					1300-2400		
Ice				0.81	-3.27				3.59	0.27
2 m	-0.22	0.22		0.58	-3.04	-1.03	-0.88		2.56	-0.60
4	-0.08	1.47		0.72	-1.79	-4.13	1.85		-0.53	2.12
8	-0.71	1.08		0.09	-2.18	-1.97	-0.74		1.61	-0.47
12	-0.34	1.28		0.46	-1.98	-2.27	0.19		1.31	0.47
20	-0.28	1.70		0.52	-1.55	-2.62	1.06		0.97	1.33
30	-0.62	0.63		0.18	-2.62	-2.04	0.54		1.54	0.81
40	-0.41	1.24		0.39	-2.02	-1.79	1.24		1.79	1.52
50	-0.94	1.55		-0.13	-1.71	-3.00	1.27		0.59	1.54
70	0.19	2.04		1.00	-1.22	-1.03	2.89		2.55	3.16
100	-0.16	2.34		0.64	-0.91	-2.98	1.74		0.61	2.02

	Relative		Time	Absolute		Relative		Time	Absolute	
	V_E	V_N		V_E	V_N	V_E	V_N		V_E	V_N
22 Apr			0100-1200					1300-2400		
Ice				2.47	0.24				-0.95	1.04
2 m	-0.11	-0.19		2.34	0.04	-0.48	-0.13		-1.25	0.70
4	-1.92	0.43		0.53	0.68	-2.77	0.08		-3.54	0.91
8	-1.95	0.35		0.51	0.60	-0.80	0.17		-1.57	1.00
12	-1.48	1.02		0.97	1.27	-0.57	0.18		-1.34	1.01
20	-1.60	1.24		0.86	1.49	-0.83	0.66		-1.60	1.50
30	-1.13	0.25		1.33	0.49	-0.81	0.13		-1.57	0.97
40	-0.42	0.59		2.04	0.83	-0.37	0.25		-1.13	1.08
50	-1.11	1.35		1.35	1.59	-0.94	2.40		-1.71	3.24
70	0.75	2.66		3.22	2.90	2.61	1.50		1.84	2.33
100	-0.37	2.83		2.08	3.07	1.62	7.24		0.86	8.08
23 Apr			0100-1200					1300-2400		
Ice				-0.65	3.69				-0.41	3.91
2 m	0.00	-0.70		-0.65	2.97	-0.29	-1.62		-0.70	2.28
4	-3.53	0.04		-4.19	3.73	-2.65	-2.63		-3.06	1.26
8	-0.82	-1.70		-1.48	1.97	-1.39	-3.10		-1.81	0.80
12	-1.39	-1.39		-2.04	2.29	-2.42	-2.42		-2.84	1.48
20	-1.55	-0.65		-2.20	3.03	-2.44	-2.26		-2.85	1.63
30	-0.43	-0.69		-1.08	2.98	-1.44	-1.64		-1.86	2.26
40	-0.44	-0.59		-1.09	3.09	-1.57	-1.12		-1.99	2.78
50	-1.12	0.32		-1.77	4.01	-1.86	-1.01		-2.28	2.89
70	-0.15	1.52		-0.79	5.21	-1.53	1.66		-1.95	5.58
100	-0.16	3.20		-0.81	6.89	-2.42	1.40		-2.83	5.31
24 Apr			0100-1200					1300-2400		
Ice				-3.12	3.39				-6.17	5.52
2 m	0.81	-1.09		-2.30	2.28	4.88	-1.99		-1.28	3.52
4	0.08	-2.11		-3.03	1.26	4.41	-5.86		-1.75	-0.34
8	0.70	-1.92		-2.41	1.46	5.15	-3.04		-1.01	2.47
12	0.10	-2.15		-3.01	1.22	3.84	-5.43		-2.32	0.09
20	0.19	-2.24		-2.92	1.13	3.97	-4.97		-2.19	0.54
30	0.33	-1.27		-2.78	2.11	2.54	-5.99		-3.62	-0.47
40	0.42	-1.55		-2.69	1.82	3.99	-5.14		-2.17	0.37
50	-0.38	-2.20		-3.49	1.18	3.24	-5.89		-2.92	-0.36
70	-3.72	-0.60		-6.84	2.78	-4.29	-7.11		-10.44	-1.16
100	-6.76	-8.24		-9.89	-4.85	-0.12	-14.91		-6.27	-8.96

	Relative		Time	Absolute		Relative		Time	Absolute	
	V_E	V_N		V_E	V_N	V_E	V_N		V_E	V_N
25 Apr			0100-1200					1300-2400		
Ice				-5.34	2.99				-7.34	1.53
2 m	2.49	-0.29		-2.84	2.69	3.17	0.83		-4.16	2.36
4	2.68	-3.15		-2.65	-0.15	3.82	-2.14		-2.50	-0.61
8	4.02	-0.88		-1.31	2.10	4.70	0.30		-2.63	1.83
12	3.20	-2.23		-2.13	0.75	4.63	-1.33		-2.70	0.19
20	3.26	-2.06		-2.07	0.92	4.57	-1.67		-2.76	-0.14
30	2.49	-2.60		-2.84	0.39	3.37	-2.84		-3.70	-0.76
40	3.88	-2.43		-1.45	0.55	3.80	-2.28		-3.27	-0.21
50	3.71	-3.25		-1.62	-0.26	6.21	-2.66		-0.86	-0.58
70	-	-		-	-	-	-		-	-
100	-	-		-	-	-	-		-	-

THE OCEANIC BOUNDARY LAYER AND ICE-WATER STRESS DURING AIDJEX 1972

by

Kenneth Hunkins
Lamont-Doherty Geological Observatory
Columbia University, Palisades, New York 10964

ABSTRACT

During the periods of storm and rapid ice drift, currents in the upper 15 to 25 m showed development of a modified Ekman spiral during the 1972 AIDJEX pilot study. A momentum integral method is used to evaluate ice-water stress. Maximum hourly mean stress is 1.66 dyn/cm^2. The balance of forces on the ice for cases when wind speed exceeds 5 m/sec shows a consistent pattern. Ice-water stress, air-water stress, and Coriolis force are all of the same magnitude. The pressure gradient force is, however, much smaller than these. Internal ice resistance is found as a residual from the force diagram and, during the rapid drift periods, is directed about 135° to the left of the ice drift.

The exchange of properties between the polar air and the polar water takes place across the pack ice barrier moving on the interface between atmosphere and ocean. In the case of momentum exchange, the flow is generally downward from air to water. Wind stress on the upper ice surface acts as a driving force and water stress on the lower ice surface acts as a retarding force. Momentum is transported downward from the atmosphere through the ice and into the oceanic planetary boundary layer.

One of the aims of the oceanographic program during the AIDJEX pilot experiment in 1972 was to assess this momentum exchange and measure ice-water stress in the central Arctic Ocean. For this purpose detailed current observations were made in the upper levels of the ocean from the lower ice surface through the planetary boundary layer and below it. The structure of the boundary layer and its changes with time over a period of one month were recorded. From this information the ice-water stress was calculated.

The techniques of current measurement and data reduction are described in an accompanying article in this issue of the AIDJEX Bulletin. Data averages over intervals of 12 hours are used here to minimize fluctuations due to turbulence and inertial oscillations. Over intervals of 12 hours ice drift and ocean currents are generally quite stable, so that we feel justified in treating these as equilibrium situations. Winds were light and ice drift small during much of the four weeks. Most of the drift was driven by the high winds of short-lived storms. Only selected intervals when ice and wind motion was sufficiently high were used for study here. During low winds the pattern is not so evident and is obscured by random experimental errors, but during high winds clear patterns of current structure emerge.

Current hodographs, lines connecting the tips of current vectors, are presented in Figures 1 and 2 for intervals when mean ice drift exceeded

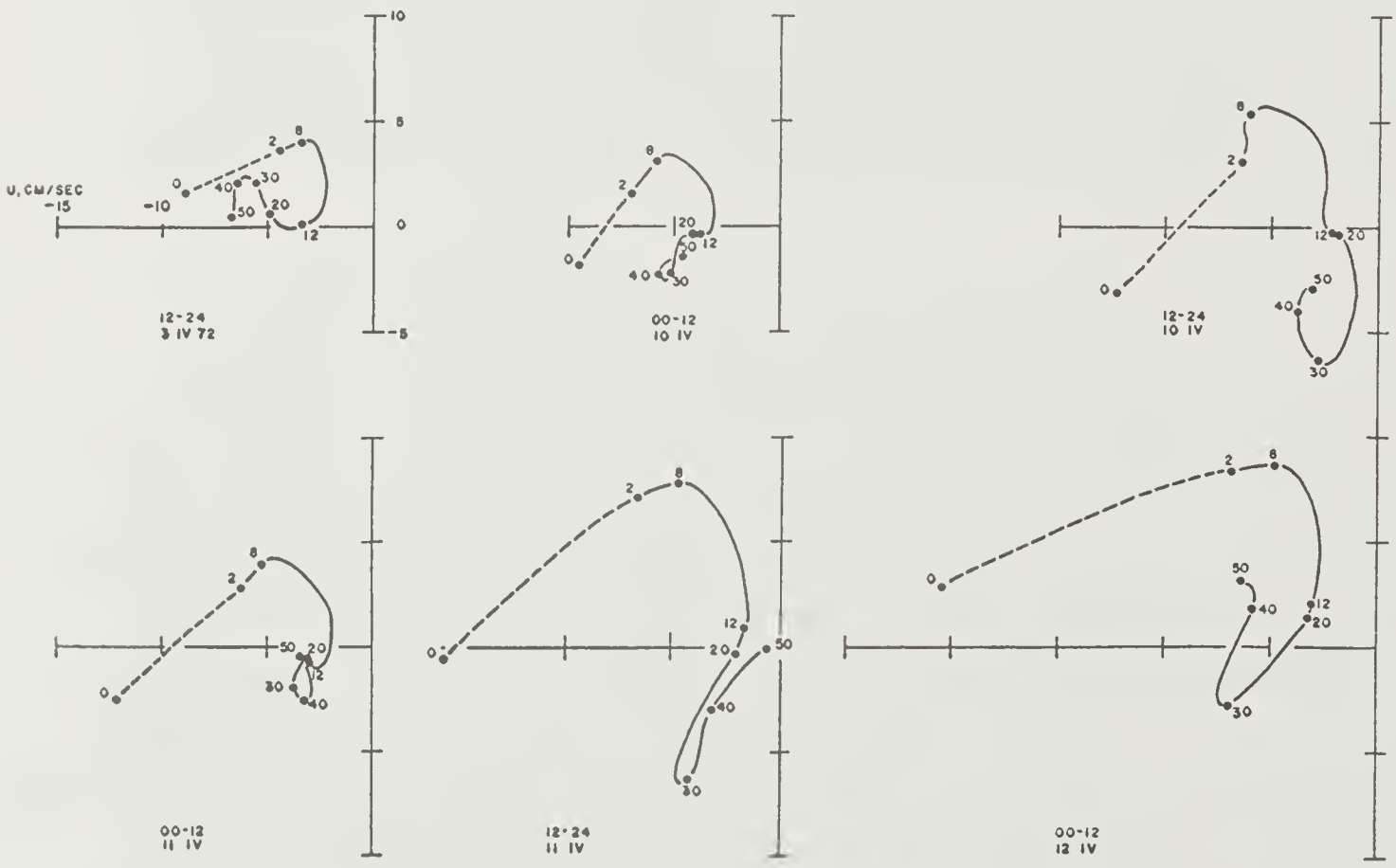

Fig. 1. Hodographs of absolute currents for 12-hour intervals with ice drift greater than 9 cm/sec. Depths in meters below ice base. North at top of page. Local standard time.

9 cm/sec. A mean hodograph over a 60-hour period coinciding with the largest storm is shown in Figure 3. The zero depth level for these measurements is the base of the ice, 2 m below sea level. The hodograph is dashed in the upper 2 m; this is considered to be the surface boundary layer in which frictional forces, but not the earth's rotation, are important. In the surface boundary layer there is a large vertical current shear in speed with very little change in current direction. Below the 2 m level there is a large current shear in both speed and direction. This is the Ekman layer, in which the effect of the earth's rotation is manifested by a clockwise rotation of the current direction. A theoretical Ekman spiral decreases exponentially downward in speed, the angle increasing in direct proportion to depth. The spiral in some of the plots tends to continue downward to 50 m. At the center of the decreasing spiral is the geostrophic current vector at the base of the Ekman layer where frictional effects vanish.

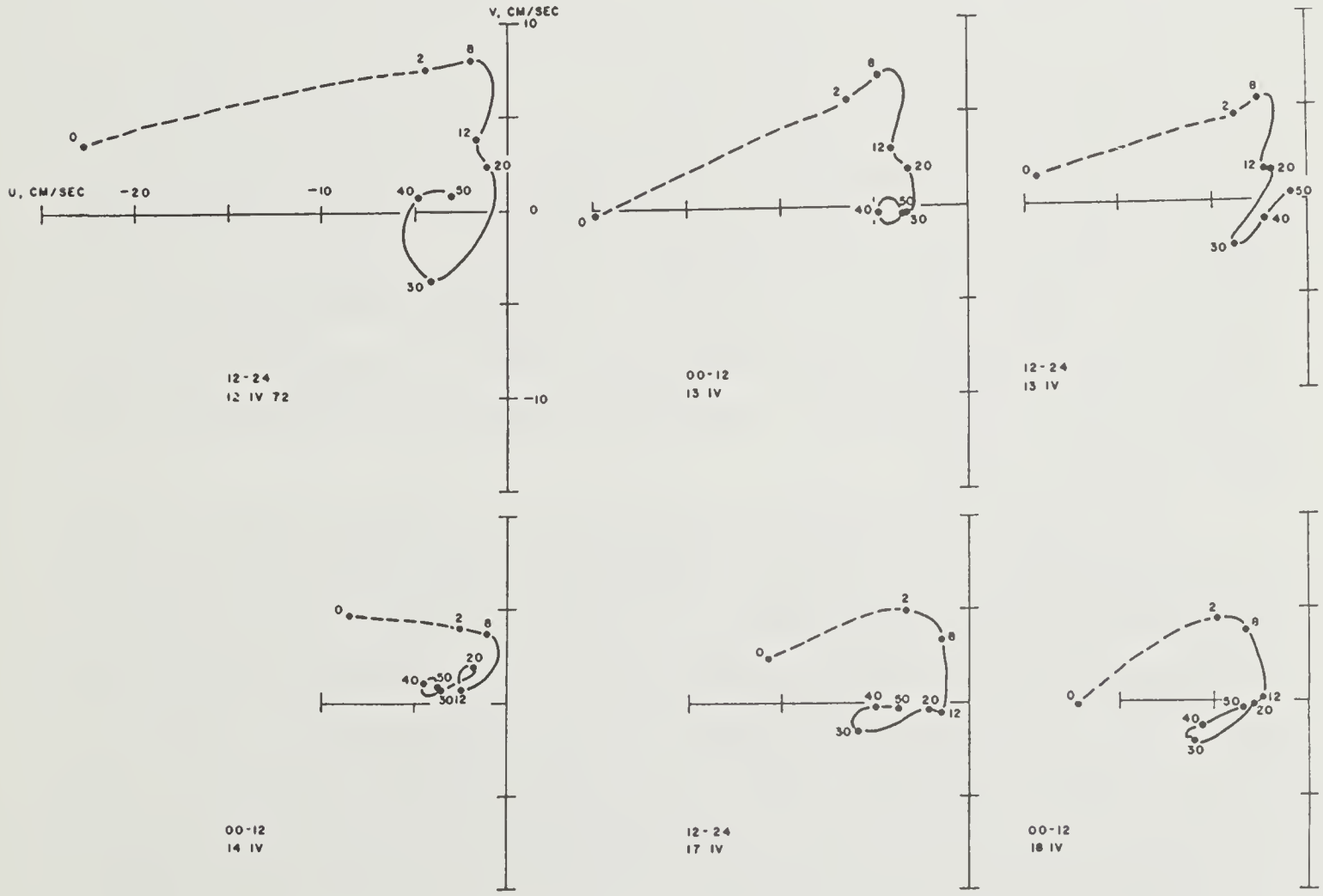

Fig. 2. Hodographs of absolute currents for 12-hour intervals with ice drift greater than 9 cm/sec. Depths in meters below ice base.

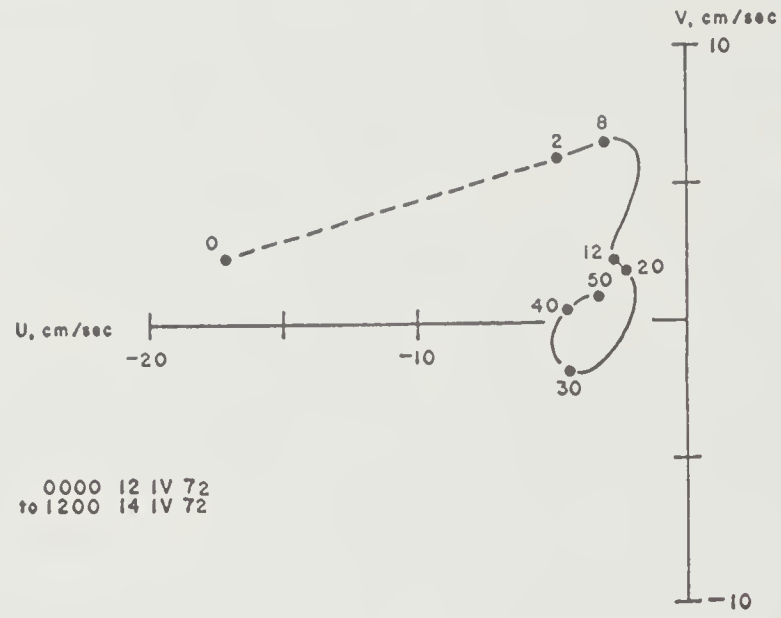

Fig. 3. Mean current hodograph for 60-hour interval during storm.

The exact depth of an Ekman spiral is not well defined since it spirals infinitely downward. Ekman took the depth to be that at which the current flowed in the direction opposite to that at the surface. Others have chosen the level at which the current speed has decreased by a factor of $1/e$ from its surface value. The exact choice is not critical for most purposes, since the speed decreases exponentially and changes are small near the base of the layer. The geostrophic current vector would lie in the center of the loop between 25 and 50 m.

The mixed layer revealed by temperature and salinity profiles during the experiment was about 35 m deep. Below this level a steep gradient in these properties and density extended to a depth of 300 m. The upper part of the mixed layer, 0-15 m, was often unstable, with brine-driven convection caused by freezing and brine production at the ice base [Smith, in press]. The lower part of the mixed layer, 15-35 m, was generally neutral or slightly stable. The Ekman layer and frictional exchange of momentum must be limited by the sharp density interface below 35 m and to some extent by the change at about 15 m.

MOMENTUM INTEGRAL METHOD

A technique involving direct evaluation of momentum in the upper water column from current profiles offers several advantages for determining ice-water stress on pack ice. Effects of both friction and form drag are included in the result. The assumptions are few, and none is made about the nature of eddy viscosity. The method can be demonstrated most simply for the case of smooth ice so that the nonlinear and pressure-gradient terms are neglected, i.e., only skin friction is acting. In the appendix it is shown that the method is more general and that with a proper set of current observations the form drag can also be included in the stress result. The horizontal equations of motion in their vertically integrated form are

$$\frac{\partial M_x}{\partial t} - f M_y = \tau_{0,x}$$

$$\frac{\partial M_y}{\partial t} + f M_x = \tau_{0,y}$$

where the mass transports are given by

$$M_x = \int_{-H}^{0} \rho(u - u_g)dz$$

$$M_y = \int_{-H}^{0} \rho(v - v_g)dz$$

with z positive upwards. It is assumed that there is a stress on the planetary boundary layer with components $\tau_{0,x}$ and $\tau_{0,y}$ at the ice-water interface but no stress at the base, $-H$, of the layer. Observed velocity components are u, v, while u_g, v_g are the geostrophic velocity components at depth $-H$, where frictional effects become negligible.

The Cartesian system used here is a valid approximation for small areas at some distance from the pole. Very close to the pole a spherical coordinate system would be necessary. A constant Coriolis parameter, f, is also a valid approximation for the relatively small areas considered.

difference. For comparison, wind stress on the upper ice surface was calculated from the synoptic observations. The drag law

$$\tau_a = \rho_a C_D V^2$$

was used with $\rho_a = 0.00125$ g/cm^3 and $C_D = 1.5 \times 10^{-3}$. The drag coefficient is based on eddy correlation measurements made with a sonic anemometer by the Bedford Institute of Oceanography group. Because of the quadratic nature of the drag law it is not strictly appropriate to use the average wind speeds. In this case, however, their use seems justified since the observed winds were fairly stationary over the 12-hour time intervals. The reverse of the wind stress direction is plotted in Figure 4 for easier comparison with water stress direction; the stresses are generally nearly opposed to each other.

Peak stresses on both top and bottom of the ice occurred during the storm of 12-13 April. It is interesting that there is a tendency for the water and wind stress to track each other fairly closely for the first day or two of a storm. After that, water stress decreases although wind stress continues to climb for another 12 hours. This pattern is also evident in the storm of 17-18 April. Maximum mean wind stress over 12 hours exceeded the water stress, reaching a maximum value of 1.875 dyn/cm^2, which coincided with a wind speed of 10.0 m/sec between 1200 and 2400 LST on 14 April. The water stress maximum of 1.101 dyn/cm^2 was attained in the preceding 12-hour interval.

BALANCE OF FORCES

During periods of strong winds, swift ice motion, and high stresses, conditions are frequently fairly stationary over 12-hour intervals and the forces acting may be considered to be in equilibrium. Information on the surface stresses of wind and water has already been presented. The body forces due to the pressure gradient associated with tilt of the ocean surface and to the Coriolis force associated with the earth's rotation must be determined. Since the current at 25 m has been assumed to be in geostrophic

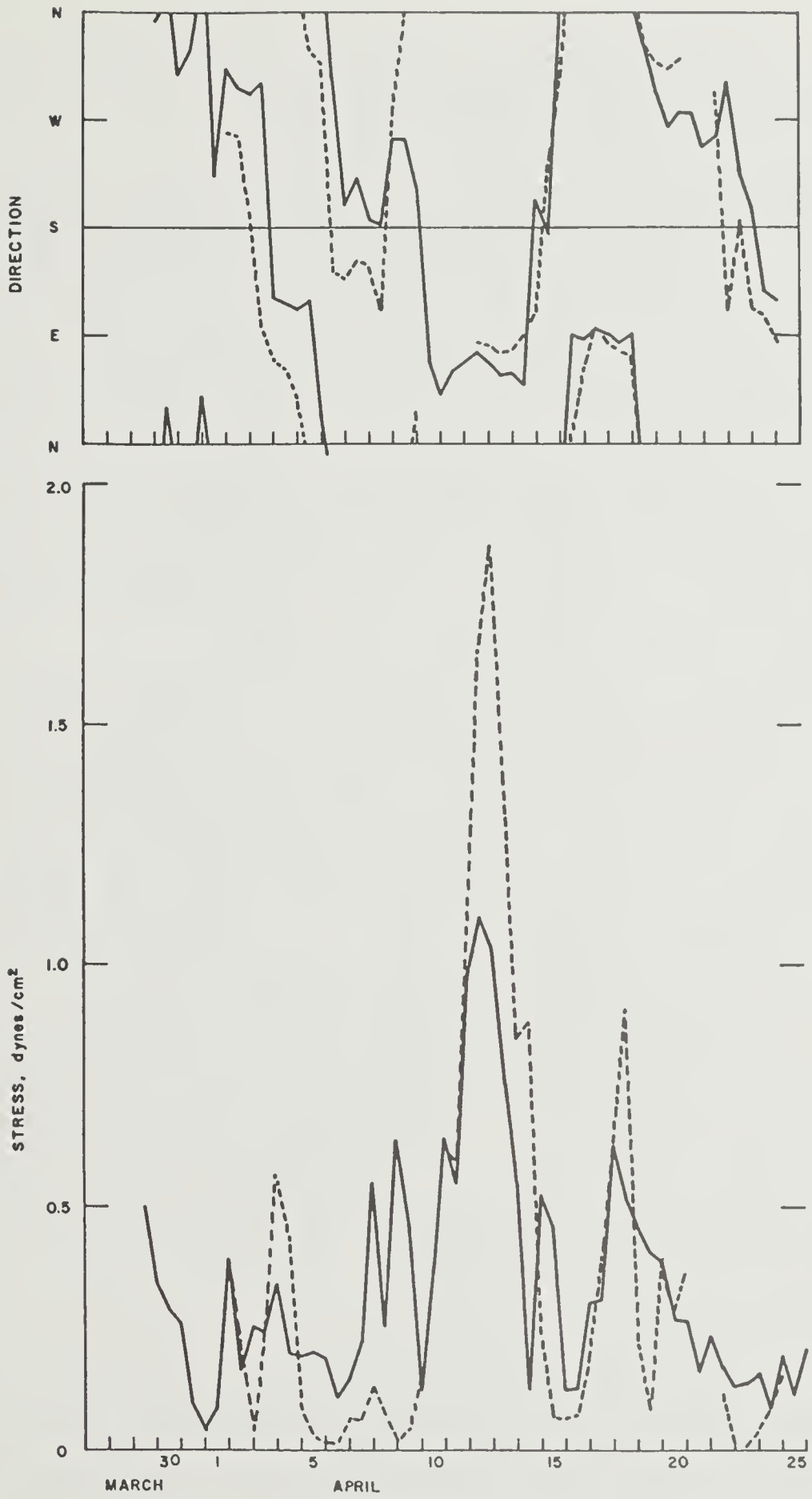

Fig. 4. Ice-water (solid line) and air-ice (dashed line) stress at 1972 AIDJEX main camp based on 12-hour means. Direction of air-ice stress reversed for comparison.

The variation of this parameter with latitude would have to be included if large areas of the earth's surface were being considered.

The geostrophic current is assumed to be barotropic, since the planetary boundary layer coincided with the upper mixed layer in the 1972 experiments so that no baroclinic currents would have been present. A uniform geostrophic current prevails through the Ekman layer. Its value is the observed current at depth $-H$. At deeper levels there is stratification and there may be vertical shear in the geostrophic current. At shallower depths the observed current is the sum of frictional and geostrophic currents. If density variations are present in the upper layer, hydrographic stations would be necessary to evaluate the baroclinic contribution to the geostrophic current, but for a well-mixed Ekman layer, current observations alone are sufficient to determine ice-water stress by the momentum integral technique.

The method depends, like any experimental method, on the quality of the observations. Sufficient measurements must be made of currents in a vertical profile and spaced closely enough in time that representative means can be formed. The available data described in the accompanying article appear to be adequate for the purpose. From the data a choice of depth, $-H$, must be made. It is evident in Figures 1 and 2 that a mean Ekman spiral exists over time periods of 12 hours. The depth $-H$ may be arbitrarily defined as the depth at which the current flows opposite to its surface direction, or it may be taken as the depth at which speed has decreased to $1/e$ of its surface value. Another approach would be to choose the depth as the first minimum in the north and east velocity profiles. At that level, mean stress would vanish. Still another approach is to examine the hydrographic profiles for the sharp density change at the base of the mixed layer and assume that this coincides with the depth of the Ekman layer. Any one or some combination of these ways of choosing $-H$ could be objectively stated so that the level could be selected individually for each profile. This may be done in the future, but for the 1972 data a constant level of 25 m was chosen for all profiles. This is approximately the level of current reversal and decrease of speed to $1/e$ of the value at 2 m relative to the geostrophic current. Since speeds are small near this level, the exact choice of depth does not seem especially critical.

An added guide to the choice of Ekman layer depth is provided by hydrographic profiles which show instability due to brine convection in the 0-15 m layer, neutral or slightly positive stability in the 15-35 m level, and strong stability below 35 m. Convection in the uppermost 15 m will mix momentum thoroughly down to this depth and possibly somewhat below it. The choice of 25 m here is in agreement with these hydrographic measurements.

The equations imply horizontal uniformity, and only a single vertical current meter array was used. Keels of pressure ridges may be expected to extend to an average depth of 10 m at an average spacing of about 200 m. Averaging over these keels is accomplished by the horizontal transport of momentum in the Ekman layer. Effects of keels upstream are carried to the observation site by advection. The distance of influence may be loosely estimated as one to two orders of magnitude of the Ekman layer thickness, that is, 250 m to 2500 m. Another estimate of distance of upstream influence can be found from the response time of an Ekman layer, which is somewhat shorter than one inertial period (12.4 hr at latitude 75°N). At 10 cm/sec a water particle travels a distance of about 2 km in one inertial period.

Ice-water stress was evaluated for the period 29 March to 25 April using hourly current values at levels of 2, 8, 12, 20, and 30 m below the base of the ice. Differences of current velocity between the geostrophic level at 25 m and shallower levels were calculated and integrated vertically using the trapezoidal rule. These are the Ekman mass transports; they assume a water density of 1.0 g/cm^3. The time-dependent term was found by taking hourly differences of these transports. The mean time-dependent term was about one order of magnitude less than the Coriolis force term. Note that only relative currents are required for finding Ekman mass transport.

Variations of stress magnitude and direction are shown in Figure 4. The maximum mean stress over 12 hours was 1.10 dyn/cm^2 for 0000-1200 LST on 12 April. The maximum mean hourly stress was 1.66 dyn/cm^2 at 0800-0900 LST of the same day. Stress results during the same period were reported as 1.0 dyn/cm^2 by the University of Washington using an eddy correlation method [Smith, in press]. The eddy correlation method gives only surface friction, and it may be that the difference between the two methods is attributable to form drag. However, the errors in the methods may account for the

balance and since the pressure gradient does not vary with depth over the top 25 m of the water column, the pressure gradient found at the base of the Ekman layer is the same as that acting on the ice. $F_{p,E} = -\rho_i h f v_g$ and $F_{p,N} = \rho_i h f u_g$ are the pressure-gradient forces in the east and north directions, respectively, where the following constants are used: ice density, $\rho_i = 0.9$ g/cm^3; ice thickness, $h = 2.5$ m; and Coriolis parameter, $f = 2\Omega \sin\phi$, where $\phi = 75°$ and Ω is the earth's angular velocity.

Note that absolute current velocities are required to find the pressure-gradient force. The Coriolis force depends only on ice velocity and is given by

$$F_{c,E} = \rho_i h f V$$

$$F_{c,N} = -\rho_i h f U$$

where U and V are components of ice velocity in the east and north directions, respectively.

These four forces are plotted for selected 12-hour intervals in Figures 5, 6, and 7 and for 60-hour intervals in Figure 8. There is also an inertial force due to the acceleration of the ice, but this term is negligible in the present cases, being too small to plot. The eight cases in these figures are for intervals when mean wind speed exceeded 5 m/sec. With the constants used, this is equivalent to cases when wind stress exceeded 0.5 dyn/cm^2. The velocity of the ice is plotted also in these diagrams, although it does not enter into the balance of forces. If it is assumed that the ice is drifting under balanced forces, then an equilibrant is required for balance. This fifth force, not measured directly but determined as a residual, is the internal ice force.

The diagrams indicate that all forces except the pressure-gradient are generally significant. However, on longer time scales, pressure-gradient forces may assume more significance. Over a mean drift of one month for AIDJEX 1972 the Coriolis and pressure-gradient forces are nearly balanced [Newton and Coachman, 1973].

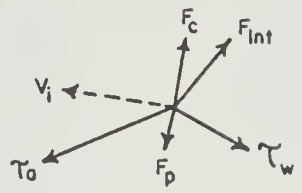

12-24
3 IV 72

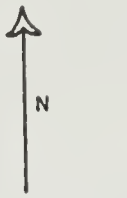

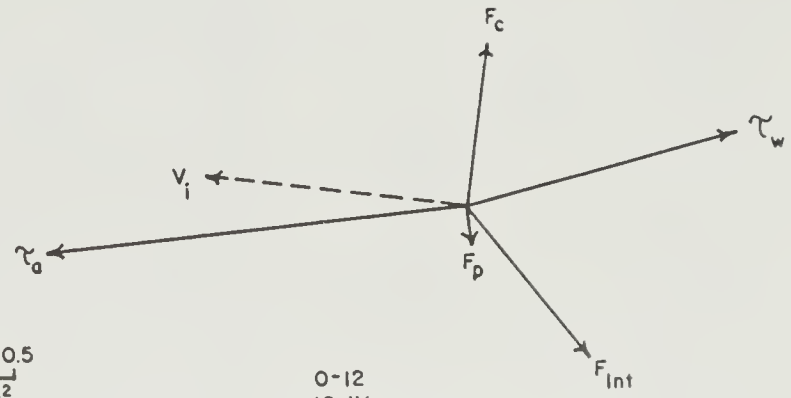

0-12
12 IV

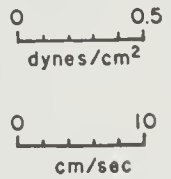

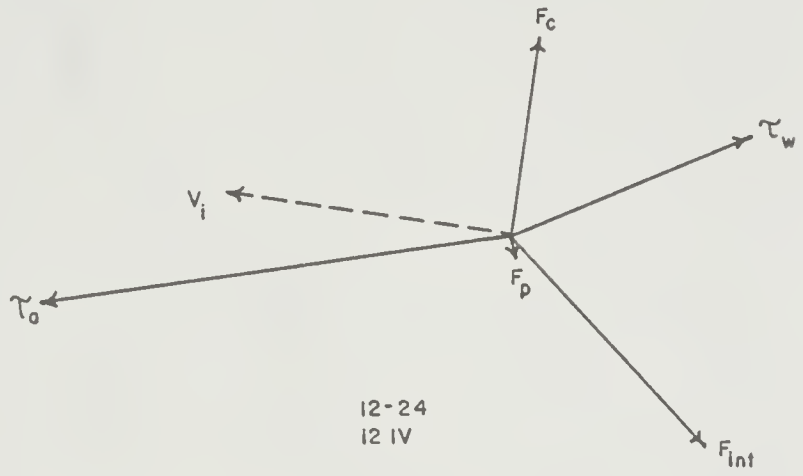

12-24
12 IV

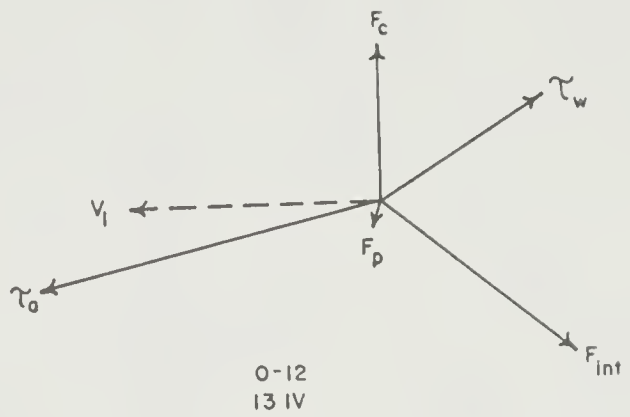

0-12
13 IV

Fig. 5. Balance of forces on ice for 12-hour intervals when winds exceeded 5 m/sec. Ice velocity, V_i, in cm/sec; air-ice stress, τ_a; ice-water stress, τ_w; Coriolis force, F_c; pressure-gradient force, F_p; and internal ice force, F_{int}.

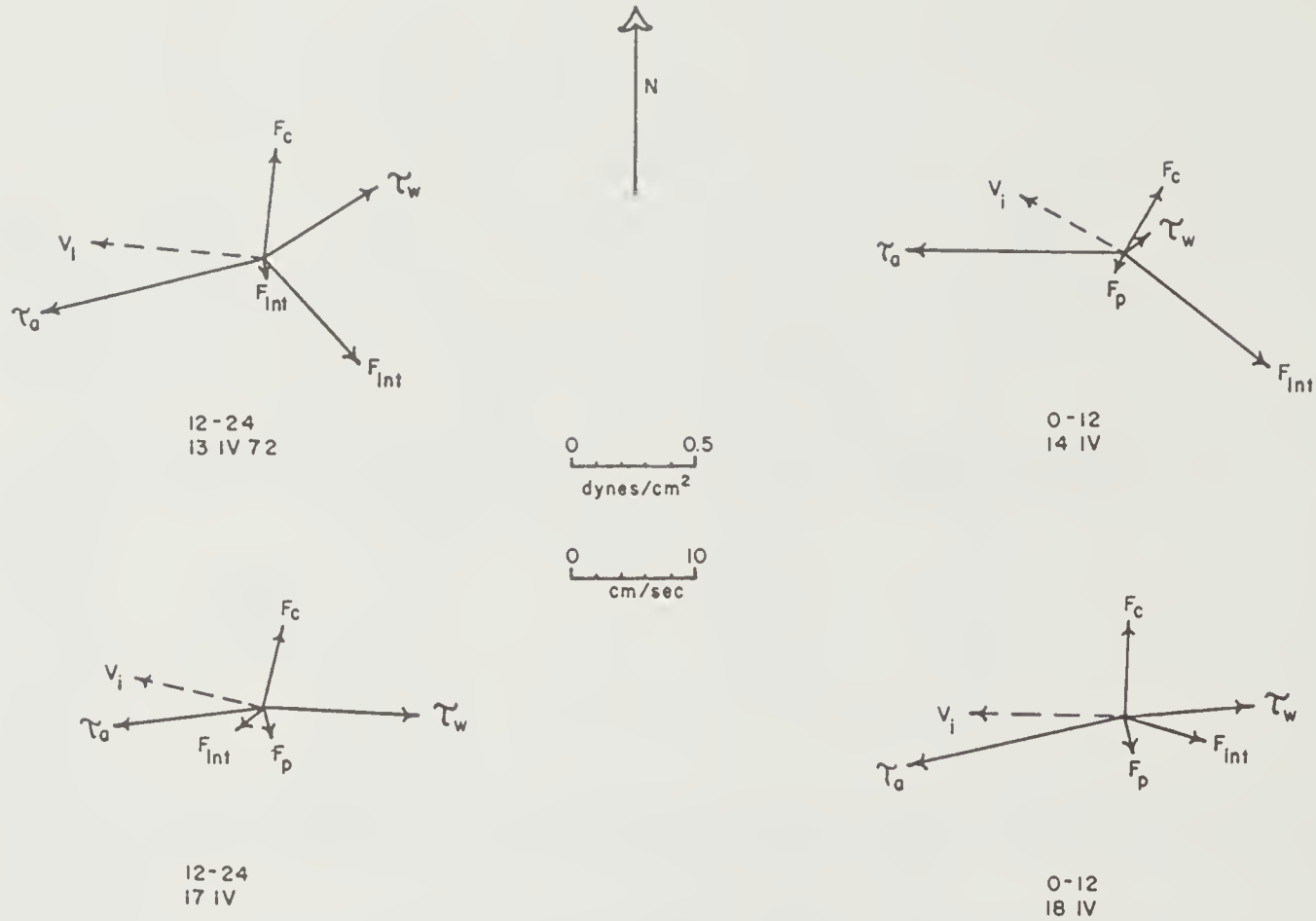

Fig. 6. Balance of forces on ice for 12-hour intervals when winds exceeded 5 m/sec. Ice velocity, v_i, in cm/sec; air-ice stress, τ_a; ice-water stress, τ_w; Coriolis force, F_c; pressure-gradient force, F_p; and internal ice force, F_{int}.

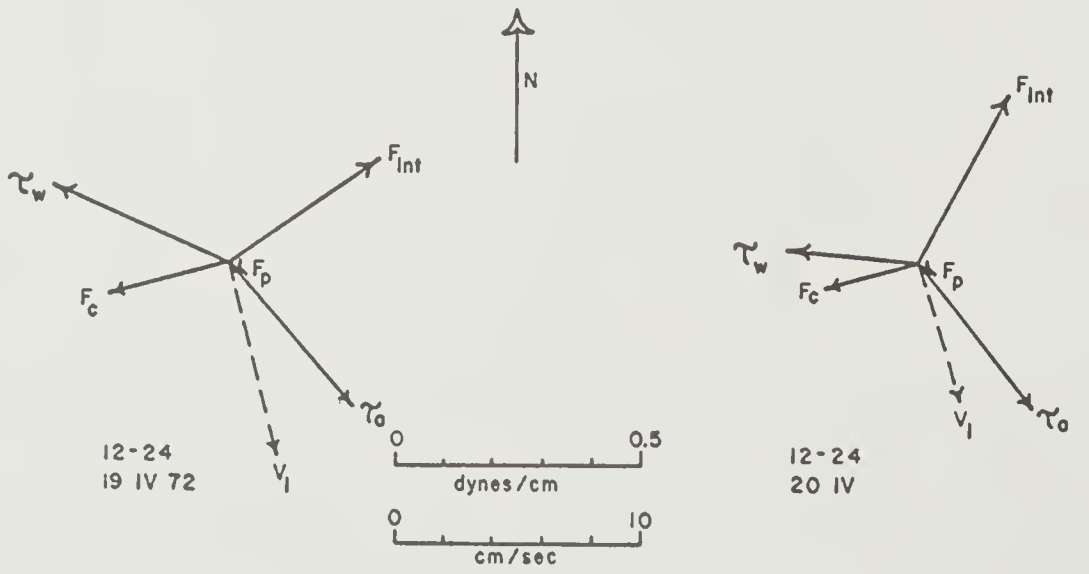

Fig. 7. Balance of forces for two cases with westerly winds.

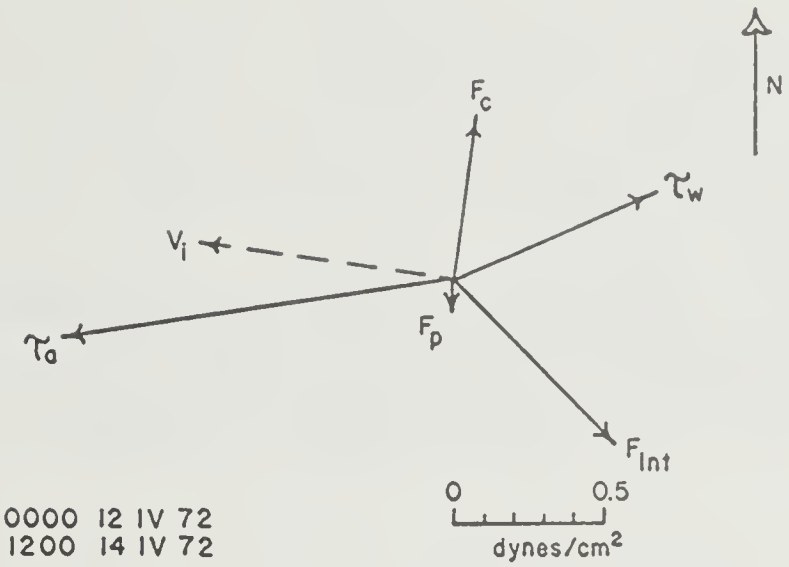

Fig. 8. Balance of forces for 60-hour interval.

The pattern of stresses is consistent during the highest values of stress (Fig. 5). During some lower values of stress (Fig. 6), deviations from the earlier pattern are seen. The consistency of the pattern during the highest stresses suggests that random errors are not a problem and that averaging in time and space is adequate. The presence of systematic errors is not ruled out, however. All of these were cases of easterly winds. Two cases of westerly winds were examined to see if the pattern changes with azimuth. These cases (Fig. 7) were for winds less than 5 m/sec. The force diagram still shows a similar pattern for these two cases, with air stress about 30° to the left of ice motion, water stress about 135° to the right of ice motion, and internal ice stress about 135° to the left of ice motion.

ACKNOWLEDGMENT

This research was supported by the Office of Naval Research under contract N00014-67-A-0108-0016.

REFERENCES

Faller, A. J., and K. A. Mooney. 1971. The Ekman boundary-layer stress due to flow over a regular array of hills. *Boundary-Layer Meteorology*, *2*, 83-107.

Hunkins, K., and M. Fliegel. 1974. Current observations at the main camp during the AIDJEX 1972 pilot program. In this Bulletin.

Newton, J., and L. Coachman. 1973. 1972 AIDJEX interior flow field study: preliminary report and comparison with previous results. *AIDJEX Bulletin No. 19*, 19-42.

Smith, J. D. 1974. Turbulent structure of the surface boundary layer in an ice-covered ocean. *Proc. 1972 ISES Symposium on The Physical Processes Responsible for the Dispersal of Pollutants in the Sea, with Special Reference to the Nearshore Zone. Rapports et Proces - Verbaux Series*, ed. J. W. Talbot and G. Kullenberg. In press.

APPENDIX

THE INTEGRATED STRESS ON A ROUGH SURFACE IN A ROTATING SYSTEM

Consider a rough surface, such as the underside of pack ice, moving over an ocean of great depth. Frictional effects will vanish at H, the depth of the planetary boundary layer, which in this case is small relative to the total depth of the ocean. The x-component of the Navier-Stokes equation in a local Cartesian coordinate system is

$$\frac{\partial u}{\partial t} + u\frac{\partial u}{\partial x} + v\frac{\partial u}{\partial y} + w\frac{\partial u}{\partial z} - fv = -\frac{1}{\rho}\frac{\partial p}{\partial x} + \frac{\partial}{\partial x}\tau_{xx} + \frac{\partial}{\partial y}\tau_{yx} + \frac{\partial}{\partial z}\tau_{zx} \quad (1)$$

where u, v, and w are the velocity components in the x, y, and z directions, respectively; ρ is density; p is pressure; and τ_{xx}, τ_{yx}, and τ_{zx} are the viscous stress components. The equation of continuity is

$$\frac{\partial u}{\partial x} + \frac{\partial v}{\partial y} + \frac{\partial w}{\partial z} = 0 \quad (2)$$

for uniform density conditions. We are concerned with flows on scales small enough that we may neglect the variation of f, the Coriolis parameter, with latitude. We are interested in average stress over a distance, X, sufficiently long to include a representative sample of roughness conditions. A weighting factor is defined to average horizontally across the water between solid protuberances. Average values in the x-direction of a representative dependent variable, q, are defined as

$$q(y,z,t) = \frac{1}{X}\int_{-X/2}^{X/2} a\, q(x)\,dx \quad (3)$$

The weighting factor a is unity when the position x lies within the fluid and is zero when it lies within a solid portion of the rough boundary. Perturbations from the horizontal average are defined by

$$q' = q - \overline{q} \quad (4)$$

Substituting equation 3 into equation 1 gives the perturbation equation

$$\frac{\partial}{\partial t}(\bar{u}+u') + (\bar{u}+u')\frac{\partial}{\partial x}(\bar{u}+u') + (\bar{v}+v')\frac{\partial}{\partial y}(\bar{u}+u') + (\bar{w}+w')\frac{\partial}{\partial z}(\bar{u}+u')$$

$$- f(\bar{v}+v') = -\frac{1}{\rho}\frac{\partial}{\partial x}(\bar{p}+p') + \frac{\partial}{\partial x}(\bar{\tau}_{xx}+\tau'_{xx}) + \frac{\partial}{\partial y}(\bar{\tau}_{yx}+\tau'_{yx})$$

$$+ \frac{\partial}{\partial z}(\bar{\tau}_{zx}+\tau'_{zx}). \qquad (5)$$

This equation is now averaged over x, noting that the x-average of an x-derivative gives values at the points x_{1n} and x_{2n} (Fig. 9). For example, the average of $\partial p'/\partial x$ is given by

$$\frac{\partial p'}{\partial x} = \sum_n \frac{p'(x_{2n}) - p'(x_{1n})}{X} \equiv \widetilde{\Delta p'} \qquad (6)$$

For $z < h$, the greatest protuberance depth, the partial x distance,

$$X_n(x,z) = \int_{-X/2}^{X/2} a\, dx = \sum_n (x_{2n} - x_{1n}),$$

is the distance occupied by water.

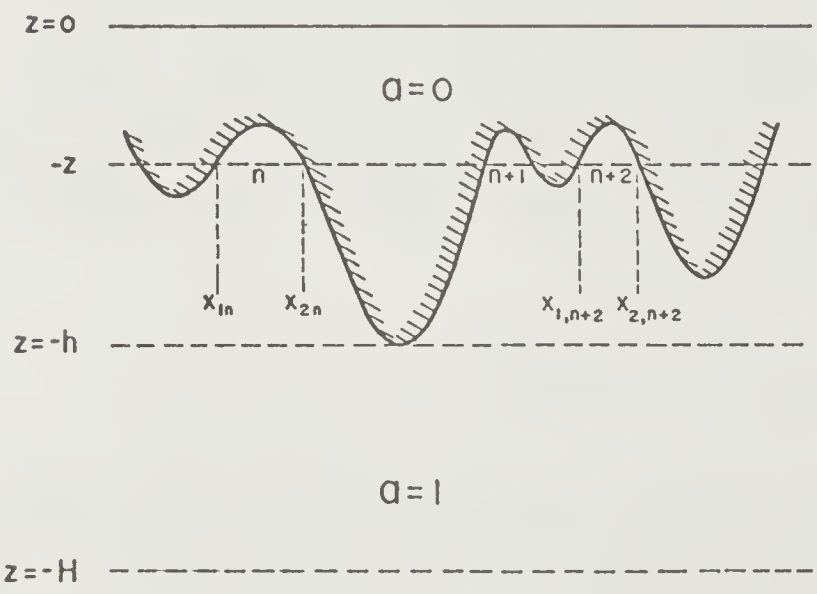

Fig. 9. Scheme for horizontal integration at constant height, z, passing through solid keels. The weighting factor a is zero within the solid and unity in the water.

The x-average of the nonlinear terms in eq. 4 can be rewritten as in the following example:

$$\begin{aligned}\overline{(\bar{v} + v')\frac{\partial}{\partial y}(\bar{u} + u')} &= \overline{\bar{v}\,\frac{\partial \bar{u}}{\partial y}} + \overline{v'\,\frac{\partial \bar{u}}{\partial y}} + \overline{\bar{v}\,\frac{\partial u'}{\partial y}} + \overline{v'\,\frac{\partial u'}{\partial y}} \\ &= \bar{v}\,\frac{\partial \bar{u}}{\partial y} + \overline{v'}\,\frac{\partial \bar{u}}{\partial y} + \bar{v}\,\frac{\partial \overline{u'}}{\partial y} + \overline{v'\,\frac{\partial u'}{\partial y}} \\ &= \bar{v}\,\frac{\partial \bar{u}}{\partial y} + \overline{v'\,\frac{\partial u'}{\partial y}}\end{aligned} \tag{7}$$

since $\overline{u'} = \overline{v'} = 0$ by definition. Thus the left-hand side of equation 4, averaged over x, becomes

$$\frac{\partial \bar{u}}{\partial t} + \bar{u}\,\frac{\partial \bar{u}}{\partial x} + \bar{v}\,\frac{\partial \bar{u}}{\partial y} + \bar{w}\,\frac{\partial \bar{u}}{\partial z} + \overline{u'\,\frac{\partial u'}{\partial x}} + \overline{v'\,\frac{\partial u'}{\partial y}} + \overline{w'\,\frac{\partial u'}{\partial z}}$$

but

$$\begin{aligned}u'\,\frac{\partial u'}{\partial x} + v'\,\frac{\partial u'}{\partial y} + w'\,\frac{\partial u'}{\partial z} &= \frac{\partial (u'u')}{\partial x} + \frac{\partial (u'v')}{\partial y} + \frac{\partial (u'w')}{\partial z} \\ &\quad - u'\left(\frac{\partial u'}{\partial x} + \frac{\partial v'}{\partial y} + \frac{\partial w'}{\partial z}\right).\end{aligned} \tag{8}$$

Substitution of the perturbation velocity values into the equation of continuity (2) shows that the last term in parentheses in eq. 8 is zero.

Equation 5 in x-averaged form then becomes

$$\begin{aligned}\frac{\partial \bar{u}}{\partial t} + \bar{v}\,\frac{\partial \bar{u}}{\partial y} + \bar{w}\,\frac{\partial \bar{u}}{\partial z} - f(\bar{v} - v_g) &= -\frac{1}{\rho}\,\widetilde{\Delta p'} + \widetilde{\Delta \tau'_{xx}} + \frac{\partial}{\partial y}\left[\bar{\tau}_{yx} - \overline{v'u'}\right] \\ &\quad + \frac{\partial}{\partial z}\left[\bar{\tau}_{zx} - \overline{w'u'}\right]\end{aligned} \tag{9}$$

The large-scale pressure gradient has been separated out as the geostrophic velocity, v_g. The remaining pressure term is associated only with form drag.

Note that the no-slip boundary condition requires that the term $\frac{\partial}{\partial x}\,(u'u') = 0$.

The $\frac{1}{\rho}\,\widetilde{\Delta p'}$ term represents the net pressure drag across the protuberances, and the $\widetilde{\Delta \tau'_{xx}}$ term represents the net effect of asymmetries in the fluctuating gradient $\partial u'/\partial x$ evaluated at positions x_{1n} and x_{2n}. The last two terms on the right-hand side of eq. 9 are the horizontally integrated effects of skin friction, including both viscous and turbulent contributions.

Assume now that the variation in the y-direction of the average parameters, $\bar{u}$, $\bar{\tau}_{yx}$, and $\overline{v'u'}$, is negligible. This implies that conditions are laterally uniform. Also assume that $\bar{w} = 0$. Vertical motion is zero at the upper boundary surface which is rigid, and this condition implies that vertical motion vanishes also at the base of the planetary boundary layer. Ekman divergence effects which can induce vertical velocity at the base of the layer are thus neglected.

Equation 9 is integrated vertically from the base of the planetary boundary layer, $-H$, where geostrophic velocities, u_g and v_g, exist upward to the rough surface:

$$\frac{\partial M_x}{\partial t} - f M_y = \int_{-h}^{0} X_n(\rho \widetilde{\Delta\tau'_{xx}} - \widetilde{\Delta p'})dz + \int_{-H}^{0} X_n \frac{\partial}{\partial z}[\bar{\tau}_{zx} - w'u']dz \quad (10)$$

where X_n is the horizontal weighting factor and the horizontal mass transports are given by

$$M_x = \rho \int_{-H}^{0} X_n(\bar{u} - u_g)dz$$
$$M_y = \rho \int_{-H}^{0} X_n(\bar{v} - v_g)dz \quad (11)$$

Only the velocity departure from the geostrophic is used in the case of M_x as well as M_y. Since the time rate of change of M_x is involved, adding a nearly constant geostrophic velocity does not affect the result. Since density is constant, the geostrophic velocities do not vary with depth.

The assumption of vanishing stress at the depth $-H$ allows the lower limit of integration in the second integral to be reduced from $-H$ to $-h$. The right-hand side of eq. 10 sums the contributions from turbulent and roughness asymmetries, pressure drag, and skin friction due to both molecular viscosity and turbulent contributions. These effects may be combined into a single integrated boundary stress term with components $\tau_{0,x}$ and $\tau_{0,y}$ so that eq. (11) becomes

$$\frac{\partial M_x}{\partial t} - f\, M_y = \tau_{0,x}$$

$$\frac{\partial M_y}{\partial t} + f\, M_x = \tau_{0,y} \qquad (12)$$

where the y-equation has been obtained in an analogous manner to the x-equation. Thus the total stress on a rough surface in a rotating system may be determined from the mass transports in the planetary boundary layer which have been averaged over a representative horizontal distance. Equation 12 is a statement of the Ekman transport relation including time dependence and with the added generalizaiton that the stress term includes both skin friction and form drag. Vertical integration has freed the result from dependence on the details of flow structure and friction within the Ekman layer.

This derivation is similar to one given by Faller and Mooney [1971] for Ekman boundary layer stress over a rough surface in a rotating tank.

Application of the method requires that the mass transports be averaged over a representative area. Provided that the averaging is adequate, the method will be rigorous even though the protuberances penetrate a large fraction of the planetary boundary layer. In practice, measurements at only a single location have been used for measuring stress below pack ice. This is justified provided that the site is located at an average ice thickness so that no weighting of the velocity values is required and provided that the protuberances are not so deep as to cause extreme variations from one location to another. Camp sites are normally chosen away from large ridges in areas of fairly level ice; this choice is suitable for the method. Details around large ridges are ignored, and for this reason the momentum integral method tends to underestimate drag.

AN ESTIMATE OF INTERNAL WAVE DRAG ON PACK ICE

by

Kenneth Hunkins
Lamont-Doherty Geological Observatory
Columbia University, Palisades, New York 10964

ABSTRACT

As pack ice drifts in a stratified ocean, the deep keels of pressure ridges generate internal waves which produce a retarding force on the motion. An estimate of this drag force was made by scaling results from experiments performed long ago by Ekman, who towed ship models in a tank with two fluid layers of different densities. For conditions assumed to be typical of the Arctic Ocean, internal wave drag is shown to amount to only 10% of the form drag and only 20% of the skin friction. The two-layered model gives only the effect of one mode. Further studies with multiple layers or with continuous stratification would be valuable to find the drag contribution of higher modes.

The resistance of fluids to moving bodies can usually be divided for descriptive and measurement purposes into three types. *Skin drag* is caused by the velocity shear near the surface of the body. *Form drag* is due to the turbulent wake which occurs after the boundary layer has separated from the surface. Both of these types of drag are a function of velocity, usually squared, with a proportionality constant known as the drag coefficient. Both types of drag have been discussed and measured to some extent on pack ice.

If the fluid has a free surface, a third type of resistance, *wave drag*, may also exist. The loss of energy to the train of gravity waves left behind the object produces drag. Surface wave drag is not important in pack ice where nearly total ice cover prevents the generation of waves on the surface. However, if a fluid is composed of layers with differing densities, internal waves may be generated that can also produce wave drag. Like most oceans, the Arctic Ocean does possess density stratification. Since internal waves

and pack ice both have similar speeds it is possible that the movement of pack ice with deep keels might generate significant internal waves. Little attention has been given to this type of drag on pack ice. This note attempts to provide an estimate for wave drag on pack ice by scaling the results of model experiments.

The first studies of internal wave drag were prompted by the "dead water" resistance met by ships under certain conditions. The effect of internal wave drag on ships is evident at low speeds of about one knot, and in areas where a thin layer of fresh water overlies salt water. Thus it was especially noticeable in the time of slow sailing ships and in areas, such as the Norwegian fjords, where a fresh layer often overlies a more saline layer. Ships caught in dead water were held to the internal wave speed unless they could break free by suddenly increasing their speed. Such a sudden increase is generally possible for motor ships but not for sailing ships.

At the suggestions of Nansen and Bjerknes, Ekman [1906] undertook an extensive study of dead water. Nansen became interested in the subject when, in 1893 off the Taimur Peninsula, the *Fram* was caught by dead water that reduced the ship's speed from a normal 5 knots to 1 knot. Ekman cited this and many other examples of dead water in an historical summary, and he conducted a series of carefully organized, quantitative experiments which proved conclusively that the high resistance was due to internal waves. In these experiments, ship models were towed in tanks containing a fresh water layer over a salty layer, and the towing resistance was measured as a function of such parameters as speed, layer densities and depths, and hull shape and size.

The atmosphere is also stratified and internal waves frequently develop in the lee of mountain ranges. Lee waves, or mountain waves, are sometimes made visible by cloud bands at the wave crests which remain stationary with respect to the ground despite the wind. Reviews of the subject have been given by Miles [1969] and Turner [1973]. Although a considerable amount of theoretical work and some model studies have been stimulated by the atmospheric problem, the application of the results to the

present problem is not clear. Model studies by Davis [1969], for example, do not show good agreement with theory. The careful model studies by Ekman are still, despite the time that has elapsed, a good starting point for an estimate of internal wave drag on pack ice.

Ekman used models of the *Fram* on 1/100 and 1/200 scales as well as other hull shapes. He demonstrated that the results from one *Fram* model could be applied to the other by using the rule of Froude for ship modeling. He also showed that the results could be scaled to give results in close agreement with experience for the full-scale *Fram*. Froude's rules are based on dimensional considerations and neglect the viscosity. They were originally applied to surface wave resistance, which is the most important drag factor at higher speeds for displacement hulls.

Ekman extended the rules to cover internal wave drag. The scaling in the case of wave drag is in terms of the Froude number (F), the ratio of ship speed to the speed of long gravity waves, rather than the Reynolds number (R). The drag force is proportional to the displacement of the hull, or cube of linear increase in dimensions, and to the difference in specific gravity between the layers. This allows some of Ekman's major results to be summarized by a plot of normalized drag force versus Froude number, with the ratio of layer to keel depth as a parameter (Fig. 1).

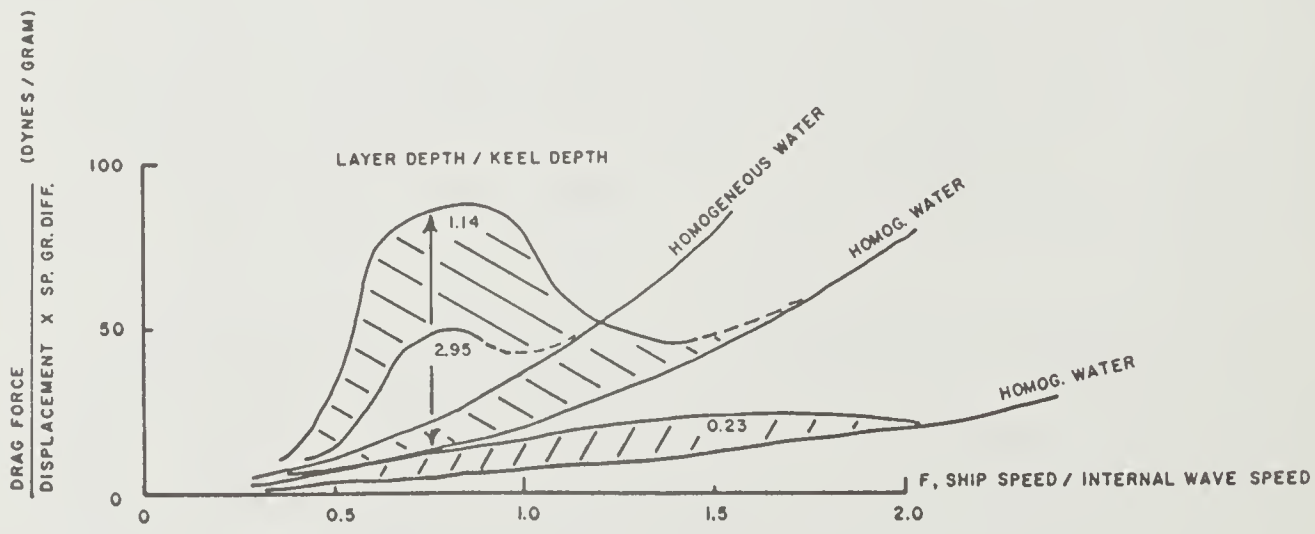

Fig. 1. Normalized internal wave drag versus Froude number with the ratio of layer to keel depth as a parameter. Curves are based on Ekman's [1906] experiments.

Drag results for homogeneous water are also shown for each keel depth. The difference between the homogeneous water curve and the appropriate curve in stratified water represents the drag due to internal waves. Two important aspects of internal wave drag are shown clearly in the figure. First, there is a maximum drag when the Froude number is 0.73, that is, when the boat speed nearly coincides with the internal wave speed. For the case of keel depth less than layer depth, wave drag is greatest for Froude numbers less than one. At that speed the largest waves are generated and drag is highest. Internal wave drag is significant only between Froude numbers of roughly 0.3 and 2.0. Note that for Froude numbers exceeding 0.73 there is an unstable region in which drag decreases as speed increases. In this speed range, ships break free of dead water, increasing their speed suddenly until limited by other types of drag. Second, the curves of Figure 1 show the effect of changing keel depths in relation to the depth of the fresh water layer. Maximum drag occurs when the keel depth is the same as the depth of the fresh water layer.

These curves may be applied to the drag of pack ice provided that layer depth, specific gravity difference, and displacement of the ice keel are known. Data are available that allow one to make reasonable estimates of these parameters. The assumptions are that the shape of the ice keel resembles a boat hull, a round-bottomed one in the case of Figure 1, and that the Arctic Ocean stratification can be represented by a density discontinuity.

Although probably only the keels of old pressure ridges resemble the hulls of ships very closely, the exact form may not be particularly critical for an estimate of internal wave drag. The different hull shapes that Ekman tested showed no remarkable differences in drag. A study by Kovacs et al. [1972] of an old pressure ridge with a keel depth of 13 m showed a smooth, roughly semicylindrical underwater form somewhat resembling a ship's hull. Younger ridges are more likely to be composed of jumbled, unconsolidated blocks with a greater form drag than old ridges, although even in this case internal wave drag may not be affected much.

Although stratification in the Arctic Ocean is actually gradual, its representation by a discontinuity is a reasonable first approximation so long

as only the first mode is being considered. A density profile taken at the AIDJEX main camp in 1972 (Fig. 2) shows a low salinity mixed layer 35 m deep overlying a steep density gradient extending to a depth of 300 m. Below the gradient lies nearly homogeneous water extending to the bottom, which is at 3800 m in this area.

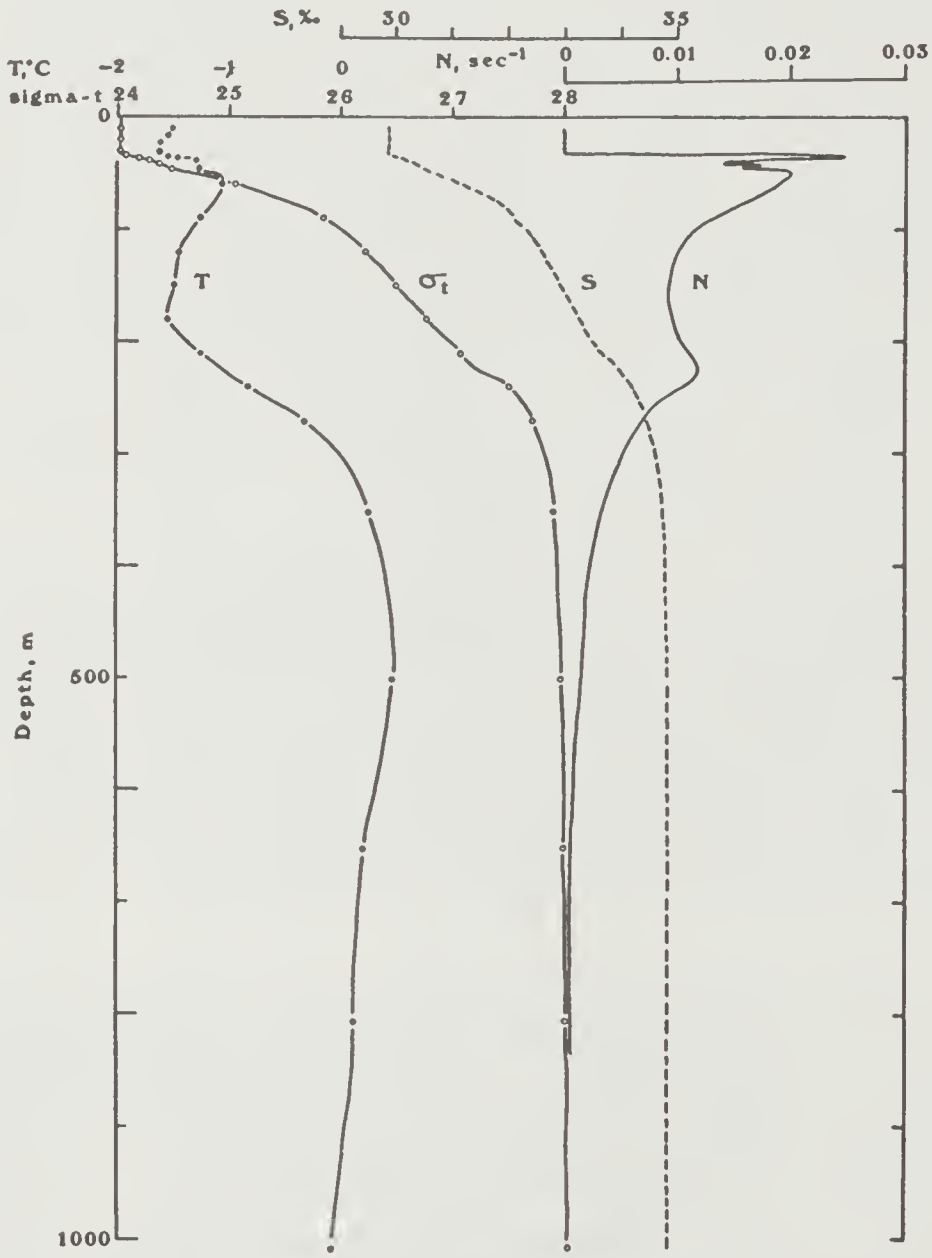

Fig. 2. Vertical profile of temperature (T), salinity (S), density (σ_t) and Väisälä frequency (N), 25 March 1972, 72°07'N 149°00'W, University of Washington hydrographic stations 24 and 26.

Internal wave dispersion curves based on this profile are shown in Figure 3. The curves are based on a matrix method for calculating internal wave properties in a rotating ocean with many layers (Fliegel and Hunkins, in preparation). Note that over the nearly level portion of the curve, phase velocity and group velocity are nearly equal. It is in this region that internal wave drag is greatest. The appropriate modeling parameter in this case is the phase velocity, which is about 200 cm/sec over the level part of the curve for the first mode.

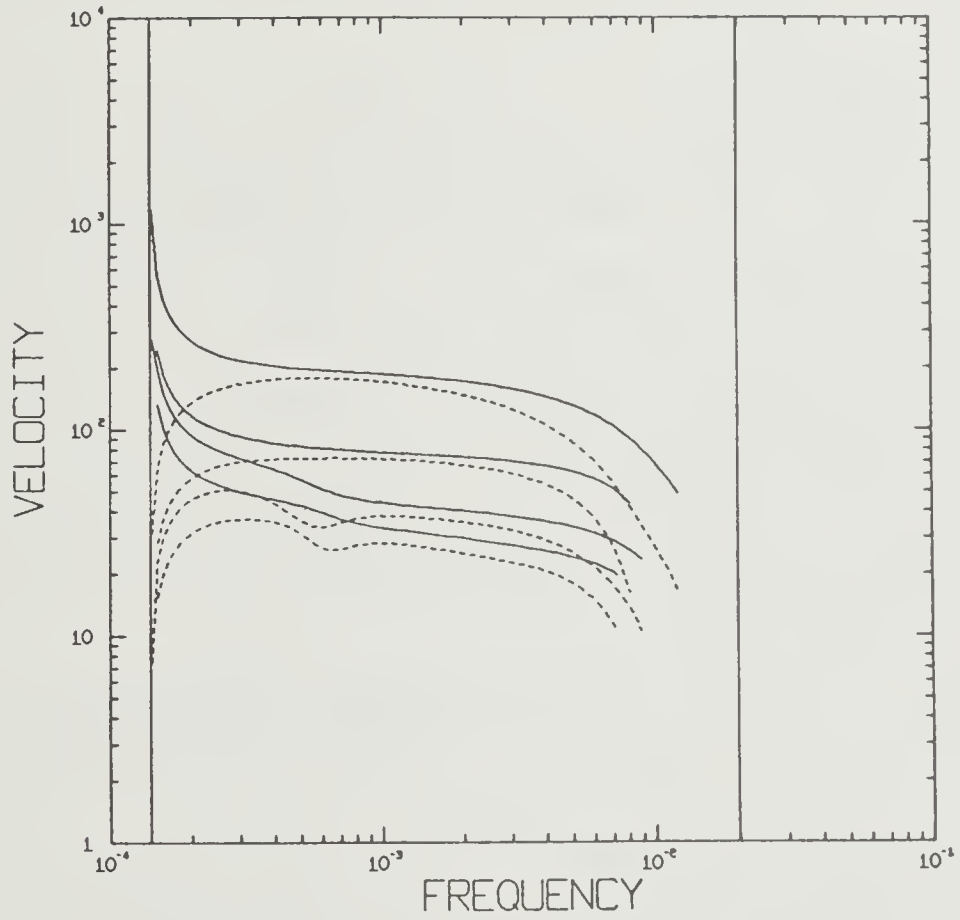

Fig. 3. Internal wave dispersion curves for the first four modes. Calculations are based on an 18-layer model approximating the density curve of Fig. 1. Solid lines are phase velocity; dashed lines are group velocity.

A two-layer model has only one mode; it is equivalent to the first mode of a multilayered model. For the two-layer model, the interface is chosen near the center of the gradient at a density of 1.026 g/cm^3. The upper layer h is 100 m thick with a density (ρ_1) of 1.024 g/cm^3, and the deep layer is in effect

infinitely thick with a density (ρ_2) of 1.028 g/cm^3. The phase velocity is

$$C = \sqrt{\frac{\rho_2 - \rho_1}{\frac{1}{2}(\rho_1 + \rho_2)}\, g\, h} = \sqrt{\frac{1.028 - 1.024}{1.026}} \times 983 \text{ cm/sec}^2 \times 100 \text{ m}$$

$$= 195.8 \text{ cm/sec},$$

where g is the acceleration due to gravity. This is sufficiently close to the multilayered model. Some experiments that Ekman performed on multiple layers showed a change of 14% at most when the density change occurred in several steps rather than in a single discontinuity.

Information on the numbers and average depths of ridge keels comes from U. S. Navy nuclear submarines whose upward-looking sonars give profiles of the bottom of the ice [Lyon, 1961]. Actual keel depths range up to 47 m, the deepest yet observed [Hibler et al., 1972]. The use of an average keel depth appears justified for rough estimates since the drag is approximately proportional to depth over the range of interest. For the central Arctic Ocean an average keel depth is taken to be 10 m with a spacing between ridges of 200 m. The ratio of layer depth to keel depth is thus 10 for the Arctic Ocean. Since the largest ratio tested by Ekman was 2.95, his data must be extrapolated.

The maximum drag appears to be approximately proportional to the reciprocal of this ratio for the range of interest. For a layer/keel depth ratio of 1.14, the maximum internal wave drag, shown by the double-headed arrow, is 72 dyn/g at a Froude number of 0.73. This is multiplied by a factor of 0.1 to compensate for the increased ratio of layer-to-keel depth in the Arctic Ocean, giving 7.2 dyn/g. Assume an increase of 200 in linear dimensions over the 1/100 *Fram* model: the actual *Fram* is 35 m × 11.5 m × 4.4 m; the model ridge is therefore 70 m long, 23 m wide, and 8.8 m deep and travels in the direction of the long axis. The 70 m long ridges would seem to occupy a large fraction of the pack. Actually a shorter hull with the same draught and width might give a similar internal wave drag. In other words, the internal wave drag may not be particularly sensitive to hull length. The actual *Fram* displaces 800 tons, and so the model ridge displaces 2^3, or 8 times, that value. Scaling the drag we have

$$D_{wave} = 7.2 \text{ dyn/g} \times 8 \times 800 \times 10^6 \text{ g} \times 0.004 = 1.84 \times 10^8 \text{ dyn}$$

Consider an ice pack with one of these ridges spaced at 200 m intervals. The internal wave stress will be

$$\tau_{wave} = \frac{1.84 \times 10^8 \text{ dyn}}{(200 \text{ m})^2} = 0.46 \text{ dyn/cm}^2$$

This represents an extreme upper limit, since the drift speed necessary to attain this value is never reached in nature. This maximum value of internal wave stress is achieved at an ice speed of

$$V_{ice} = F \times \text{internal wave speed} = F \times \sqrt{g \times \text{sp. gr. diff.} \times \text{layer depth}}$$

$$= 0.77 \sqrt{980 \text{ cm/sec}^2 \times 0.004 \times 100 \text{ m}}$$

$$= 0.77 \times 198 \text{ cm/sec} = 152 \text{ cm/sec} \simeq 3 \text{ kt}$$

This is far in excess of actual ice speeds. During the 1972 AIDJEX program, the highest observed speed was 26 cm/sec, or about 1/2 knot. This is equivalent to a Froude number of 0.13. Reference to Figure 1 shows that internal wave effects are becoming negligible at this speed. Ekman's experiments did not extend to such small Froude numbers. Extrapolation of the curve suggests that the internal wave drag is at least an order of magnitude smaller at $F = 0.13$ than at its maximum value. Thus under actual conditions, a maximum value is $\tau_{wave} \simeq 0.05 \text{ dyn/cm}^2$.

The internal wave drag must be compared with skin and form drag to determine its relative significance. In terms of Prandtl's boundary layer theory, the roughness parameter value at the AIDJEX main camp in 1972 was $z_0 = 4.17$. Assuming a reference level of $z = 2$ m, corresponding to the depth of the skin friction layer, the drag coefficient is given by

$$C_D = 2k^2/[\ln(z/z_0)]^2 = 0.021$$

where von Karman's constant, k, is 0.4. The stress due to skin friction during the period of fastest drift in 1972 was then

$$\tau_{skin} = \rho C_D u^2/2 = 1.026 \times 0.021 \times (15)^2/2 = 2.4 \text{ dyn/cm}^2$$

where u is the velocity in cm/sec. There will also be a contribution from form drag. The Reynolds number in this case will be

$$R = \rho\, ul/\mu = 1.026 \times 26 \times 10^3/10^{-2} = 2.7 \times 10^6$$

where l is a characteristic length and μ is the viscosity. Boundary layer separation has occurred for most geometric forms at this Reynolds number, and for a hemispheric shape the drag coefficient will be in the neighborhood of unity or perhaps slightly less. The form drag of a ridge will then be

$$D_{form} = \rho\, C_D\, A\, u^2/2 = 1.026 \times 1.0 \times 23\ \text{m} \times 8.8\ \text{m} \times (15)^2/2$$

$$= 2.33 \times 10^8\ \text{dyn}$$

where A is the cross-sectional area of the ridge. The stress will be

$$\tau_{form} = (2.33 \times 10^8)/(200\ \text{m})^2 = 0.6\ \text{dyn/cm}^2$$

These calculations indicate that internal wave drag on pack ice in the Arctic Ocean is negligible in comparison with other types of drag. This somewhat justifies the neglect of internal wave drag in the AIDJEX field studies where only skin and form drag have been considered.

A more precise estimate of internal wave drag on pack ice would require direct observations in the field, further model studies, theoretical investigations, or some combination of these. Theoretical investigations alone will probably not be sufficient.

The study of internal wave drag under actual conditions in pack ice presents difficulties. The internal waves that produce drag will, under steady conditions, have crests and troughs in a fixed relation to the ice. They cannot be detected from a single observation point as can internal waves generated by other causes which travel relative to the ice. Internal waves moving relative to the ice have been observed from drifting ice with thermistor strings and with echo sounders. However, either a dense horizontal net of fixed sensors or a mobile sensor is required to observe standing internal waves. The unmanned research torpedo developed by the Applied Physics Laboratory of the University of Washington would be an ideal mobile

sensor, since it could be programmed to sample along paths downstream from ridges, searching for the undulations in temperature and salinity indicative of lee waves.

A side-scanning sonar might be another useful technique. It has been shown that acoustic waves with a frequency of 100 kHz are reflected by the sharp boundary at the base of the mixed layer, which was at 35 m in 1972. A side-scanning sonar with high frequency might be able to detect the undulations of this interface over a fairly wide area and give a three-dimensional picture of it in time. Further model testing would be valuable to extend the work of Ekman to specific questions about pack ice drag. Some points to be clarified would be:

1. Drag at small ratios of layer depth to keel depth.
2. Drag at small Froude numbers.
3. Effect of shapes other than ships' hulls.
4. Effect of continuous stratification.

The calculations have been based on two-layered model tests. Although Ekman's results seemed to show otherwise, there is still a possibility that models with more layers will show high drag effects for large ratios of layer/keel depth at certain low speeds. In a two-layered model, only one mode of motion exists. The maximum of vertical motion is at the interface, which moves up and down as horizontal currents in the upper and lower layers flow in opposite directions. Higher modes with more than one maximum of vertical motion in depth may exist in fluids with many layers. The higher modes have slower phase speeds than the fundamental mode.

There may be cases in which a keel extending a small distance into the mixed layer will excite higher mode internal waves of large amplitude when it moves at a certain lower speed. Ekman's limited experiments with density gradients could have missed this effect. Note that the fourth mode has a phase velocity of 45 cm/sec in this region of high drag. It is clear that a phase speed in the range of ice speeds will occur in this flat region within the next few higher modes. These modes will have a complex vertical structure which might be excited by relatively small keels.

Vertical current shear is another complication which could be of importance. In the model tests the fluid has a uniform motion relative to the moving object. The horizontal velocity in the ocean does vary with depth during internal wave generation by pack ice. This effect has been included in various theoretical studies of lee waves in the atmosphere. The production of a flow with horizontal velocity varying in depth might require, in a tank model, considerable experimental ingenuity. Theory may be the simplest method for evaluating the importance of this particular effect.

Although there are still a number of unexamined factors, it appears that the internal wave drag generated by ridge keels is not likely to be an important factor in the general underwater resistance of ice floes in the Arctic Ocean. The assumptions and extrapolations involved in this rough analysis make it desirable to attempt more refined calculations and experiments. However, the neglect of internal wave drag relative to skin and form drag appears at present to be justifiable for large-scale ice motion.

REFERENCES

Davis, R.E. 1969. The two-dimensional flow of a stratified fluid over an obstacle. *J. Fluid Mech.*, *36*(1): 127-143.

Ekman, V.W. 1906. On dead-water. In *The Norwegian North-Polar Expedition, 1893-1896, Scientific Results*, ed. F. Nansen, *5*(15). Christiania, Norway, 1-152.

Fliegel, M., and K. Hunkins. Internal wave dispersion calculated using the Thompson-Haskell matrix method (in preparation).

Hibler, W.D. III, W.F. Weeks, and S.J. Mock. 1972. Statistical aspects of sea ice ridge distributions. *AIDJEX Bulletin No. 12*, 117-162.

Hunkins, K. 1974. Subsurface eddies in the Arctic Ocean. *AIDJEX Bulletin No. 23*. 9-36.

Kovacs, A., W.F. Weeks, S.F. Ackley, and W.D. Hibler III. 1972. A study of a multiyear pressure ridge in the Beaufort Sea. *AIDJEX Bulletin No. 12*, 17-28.

Lyon, W.K. 1961. Ocean and sea-ice research in the Arctic Ocean via submarine. *Trans. New York Acad. Sci.*, ser. 2, vol. 23, 662-674.

Miles, J.W. 1969. Waves and wave drag in stratified flows. In *Proceedings of the Twelfth International Congress on Applied Mechanics, Stanford*, ed. M. Hetenyi and W. G. Vincenti. Berlin: Springer-Verlag, 50-76.

Rigby, F. 1974. Theoretical calculations of internal wave drag on sea ice. In this AIDJEX Bulletin.

Turner, J.S. 1973. *Buoyancy effects in fluids.* Cambridge: Cambridge University Press, 31-39 and 58-63.

MANDATORY DISTRIBUTION LIST

FOR UNCLASSIFIED TECHNICAL REPORTS, REPRINTS, AND FINAL REPORTS
PUCLISHED BY OCEANOGRAPHIC CONTRACTORS
OF THE OCEAN SCIENCE AND TECHNOLOGY DIVISION
OF THE OFFICE OF NAVAL RESEARCH
(REVISED SEPT 1973)

1 Director of Defense Research
and Engineering
Office of the Secretary of Defense
Washington, D. C. 20301
Attn: Office, Assistant Director
(Research)

Office of Naval Research
Arlington, Virginia 22217
3 Attn: Code 480*
1 Attn: Code 460
1 Attn: Code 102-0S

1 ONR Branch Office
207 West 24th Street
New York, N. Y. 10011

12** Defense Doc. Center
Cameron Station
Alexandria, Va.22314

Commander
Naval Oceanographic
Office
Washington, D.C.20390
1 Attn: Code 1640
1 Attn: Code 70

1 NODC/NOAA
Bldg. 160
Washington Navy Yard
Rockville, Md.20852

1 ONR Res. Rep.
Richard Stevens

Total Required 35 copies

Director
Naval Research Laboratory
Washington, D. C. 20390
6 Attn: Library, Code 2029 (ONRL)
6 Attn: Library, Code 2620

* Add one separate copy of Form DD-1473

** Send 2 completed forms DDC-50,
one self-addressed back to
contractor, the other addressed
to ONR, Code 480

Unclassified
SECURITY CLASSIFICATION OF THIS PAGE *(When Data Entered)*

REPORT DOCUMENTATION PAGE

READ INSTRUCTIONS BEFORE COMPLETING FORM

1. REPORT NUMBER: Technical Report No. 1
2. GOVT ACCESSION NO.:
3. RECIPIENT'S CATALOG NUMBER:

4. TITLE *(and Subtitle)*:
1.OCEAN CURRENT OBSERVATIONS AT THE AIDJEX '72 MAIN CAMP.
2.THE OCEANIC BOUNDARY LAYER AND ICE WATER STRESS.
3.AN ESTIMATE OF INTERNAL WAVE DRAG ON PACK ICE.

5. TYPE OF REPORT & PERIOD COVERED: Tech.Report - one yr.

6. PERFORMING ORG. REPORT NUMBER:

7. AUTHOR(s):
1. Kenneth Hunkins and Myron Fliegel
2. Kenneth Hunkins
3. Kenneth Hunkins

8. CONTRACT OR GRANT NUMBER(s): Contract N 00014-67-A-0039

9. PERFORMING ORGANIZATION NAME AND ADDRESS:
Lamont-Doherty Geological Observatory
of Columbia University
Palisades, N. Y.

10. PROGRAM ELEMENT, PROJECT, TASK AREA & WORK UNIT NUMBERS:
NR307-359
Project No. 461

11. CONTROLLING OFFICE NAME AND ADDRESS:
Office of Naval Research and Advanced
Research Projects Agency
Code 220 - Arlington, Va. 22217

12. REPORT DATE: December, 1974

13. NUMBER OF PAGES: 152

14. MONITORING AGENCY NAME & ADDRESS *(if different from Controlling Office)*:
Office of Naval Research and Advanced
Research Projects Agency

15. SECURITY CLASS. *(of this report)*: Unclassified

15a. DECLASSIFICATION/DOWNGRADING SCHEDULE:

16. DISTRIBUTION STATEMENT *(of this Report)*:
Reproduction of this document in whole or in part is permitted for any purpose of the U. S. Government.

17. DISTRIBUTION STATEMENT *(of the abstract entered in Block 20, if different from Report)*:

18. SUPPLEMENTARY NOTES:

19. KEY WORDS *(Continue on reverse side if necessary and identify by block number)*:
Arctic Ocean
Currents
Boundary layers
Air-sea Interaction
Internal waves

20. ABSTRACT *(Continue on reverse side if necessary and identify by block number)*:
1. Ocean Current Observations at the AIDJEX 1972 Main Camp -
During the 1972 AIDJEX pilot study, mast-mounted current meters were operated continuously for 30 days in the main camp to measure currents at ten depths between 2 m and 100 m below the ice base. The currents were plotted in three forms: relative speed and direction, absolute speed and direction, and progressive vector.

DD FORM 1 JAN 73 1473 EDITION OF 1 NOV 65 IS OBSOLETE
S/N 0102-014-6601

SECURITY CLASSIFICATION OF THIS PAGE *(When Data Entered)*

2. The Oceanic Boundary Layer and Ice-water Stress During AIDJEX 1972 - During the periods of storm and rapid ice drift, currents in the upper 15 to 25 m showed development of a modified Ekman spiral during the 1972 AIDJEX pilot study. A momentum integral method is used to evaluate ice-water stress. Maximum hourly mean stress is 1.66 dyn/cm^2. The balance of forces on the ice for cases when wind speed exceeds 5 m/sec shows a consistent pattern. Ice-water stress, air-water stress and Coriolis force are all of the same magnitude. The pressure gradient force is, however, much smaller than these. INTERNAL Ice resistance is found as a residual from the force diagram and, during the rapid drift periods, is directed about 135^o to the left of the ice drift.

3. An Estimate of Internal Wave Drag on Pack Ice - As pack ice drifts in a stratified ocean, the deep keels of pressure ridges generate internal waves which produce a retarding force on the motion. An estimate of this drag force was made by scaling results from experiments performed long ago by Ekman, who towed ship models in a tank with two fluid layers of different densities. For conditions assumed to be typical of the Arctic Ocean, internal wave drag is shown to amount to only 10% of the form drag and only 20% of the skin friction. The two-layered model gives only the effect of one mode. Further studies with multiple layers or with continuous stratification would be valuable to find the drag contribution of higher modes.